[American Journal of Science, Vol. 318, May, 2018, P. 557-589, DOI 10.2475/05.2018.05]

MODEL BASED PALEOZOIC ATMOSPHERIC OXYGEN ESTIMATES: A REVISIT TO GEOCARBSULF

SHUANG ZHANG*,†, NOAH J. PLANAVSKY*, ALEXANDER J. KRAUSE**, EDWARD W. BOLTON*, and BENJAMIN J. W. MILLS**

ABSTRACT. Geological redox proxies increasingly point towards low atmospheric oxygen concentrations during the early Paleozoic Era, with a subsequent protracted rise towards present-day levels. However, these proxies currently only provide qualitative estimates of atmospheric O_2 levels. Global biogeochemical models, in contrast, are commonly employed to generate quantitative estimates for atmospheric O_2 levels through Earth's history. Estimates for Paleozoic pO_2 generated by GEOCARBSULF, one of the most widely implemented carbon and sulfur cycle models, have historically suggested high atmospheric O_2 levels throughout the Paleozoic, in direct contradiction to competing models. In this study, we evaluate whether GEOCARBSULF can predict relatively low Paleozoic O_2 levels. We first update GEOCARBSULF by adopting the recent compilation of the $\delta^{13}C$ value of marine buried carbonate and replacing the old formulation of the sulfur isotope fractionation factor with empirical sulfur isotope records. Following this we construct various O_2 evolution scenarios (with low O_2 levels in the early Paleozoic) and examine whether GEOCARBSULF can reproduce these scenarios by varying the weathering/degassing fluxes of carbon and sulfur, or carbonate $\delta^{13}C$. We show that GEOCARBSULF can, in fact, maintain low-O_2 (even 1–5% atm) levels through the early Paleozoic by only varying the carbonate $\delta^{13}C$ within 2 standard deviation (SD) bounds permitted by the geological record. In addition, it can generate a middle–late Paleozoic rise in O_2 concentration, coincident with the diversification of land plants. However, we also argue that tracking atmospheric O_2 levels with GEOCARBSULF is highly dependent on carbonate carbon isotope evolution, and more accurate predictions will come from an improved C isotope record.

Keywords: atmospheric O_2, GEOCARBSULF, Paleozoic, carbonate isotope, plant evolution

INTRODUCTION

The protracted rise of atmospheric oxygen is one of the most obvious ways in which life has reshaped our planet. However, almost all aspects of the history of atmospheric oxygen have been fervently debated over the past few decades. For instance, there is still persistent debate about the role—if any—that land plants played in driving the rise of atmospheric oxygen over the Paleozoic (Berner, 1987; Berner and Canfield, 1989; Berner, 2001; Bergman and others, 2004; Berner, 2006b; Lenton and others, 2016; Wallace and others, 2017). A series of geochemical redox proxies have been used to estimate the atmospheric O_2 levels qualitatively. Statistical analysis of iron speciation (Sperling and others, 2015) indicates widespread anoxic marine subsurface waters in the Cambrian. Cerium anomalies in well preserved marine cements and other marine precipitates confirmed that ocean anoxia was prevalent not only in the Cambrian but also through the Ordovician to Early Devonian (Wallace and others, 2017). The cerium anomaly record also argues for a continuous rise of surface O_2 levels through the Devonian, which has also been suggested by Mo isotope data (Dahl and others, 2010).

Although there are consistent advances in using geochemical paleo-redox proxies to predict O_2 levels qualitatively, quantitative estimates of atmospheric oxygen for the

* Department of Geology and Geophysics, Yale University, New Haven, Connecticut 06520, USA
** School of Earth and Environment, University of Leeds, Leeds LS2 9JT, United Kingdom
† Corresponding author email: shuang.zhang@yale.edu

Phanerozoic still come from global biogeochemical models. Over geologic time scales (>1 million years), atmospheric O_2 levels are controlled by the carbon (C) and sulfur (S) sedimentary redox cycles (Berner, 1987). Oxidative weathering of organic carbon and pyrite (and oxidation of reduced gases) will consume O_2 while sediment burial of organic carbon and pyrite will release O_2.

The representative reactions for O_2 consumption are:

$$O_2 + CH_2O \rightarrow CO_2 + H_2O \quad (1)$$

$$15O_2 + 4FeS_2 + 8H_2O \rightarrow 2Fe_2O_3 + 8SO_4^{-2} + 16H^+ \quad (2)$$

The representative reactions for O_2 release are just the reverse of the reactions above. Based on these reactions, changes in atmospheric O_2 with time can be formulated as (Berner, 2004):

$$\frac{d[O_2]}{dt} = F_{bg} - F_{wg} - F_{mg} + \left(\frac{15}{8}\right)(F_{bp} - F_{wp} - F_{mp}) \quad (3)$$

Where: F_{bg} and F_{bp} are the rate of burial of organic carbon and of pyrite sulfur in sediments; F_{wg} and F_{wp} are the rate of oxidative weathering of organic carbon and of pyrite sulfur; and F_{mg} and F_{mp} are the rate of oxidation of reduced carbon-containing gases and of reduced sulfur-containing gases released via diagenesis, metamorphism, and volcanism, respectively. The embedded ratio refers to the stoichiometry of the reaction related to pyrite formation and oxidation.

Various numeric models have been built to estimate atmospheric O_2 levels over the Phanerozoic, and these models differ in how they calculate the weathering and burial fluxes of organic carbon and pyrite (Berner and Canfield, 1989; Berner, 2001; Hansen and Wallmann, 2003; Bergman and others, 2004; Falkowski and others, 2005; Berner, 2006b; Arvidson and others, 2013; Mills and others, 2014; Lenton and others, 2016; Mills and others, 2016). The two mostly commonly utilized models for the Phanerozoic are GEOCARBSULF (Berner, 2006b; Berner, 2009) and COPSE (Bergman and others, 2004; Mills and others, 2014; Lenton and others, 2016). These models produce fundamentally different predictions for atmospheric oxygen levels over the Paleozoic. Specifically, GEOCARBSULF predicts near modern pO_2 throughout the Paleozoic (fig. 1), which implies that land plants were not essential to drive Earth to the high oxygen state characteristic of the modern world. COPSE, on the other hand, predicts low atmospheric oxygen throughout the early Paleozoic, and a rise towards modern levels during the middle-late Paleozoic coincident with the evolution of land plants (fig. 1).

These differences between models arise from the methods used to calculate O_2 fluxes: in the GEOCARBSULF model, carbon and sulfur burial rates are inverted from isotope mass balance, whereas the COPSE model calculates their burial rates based on assumed primary productivity and nutrient recycling. Primary productivity and nutrient recycling are difficult to estimate for Earth's past, especially when considering the Paleozoic where geologic data are sparse. In COPSE (Bergman and others, 2004), an increase of carbon burial on land in the Carboniferous was driven by doubling the C:P burial ratio of land organic matter to represent the effects of enhanced preservation in swamps and mires. This model condition contributes to a mid-Paleozoic O_2 rise. Similarly, the assumption of a high C:P ratio and high land primary productivity starting from ~470 Ma leads to the rapid rise of O_2 in the early Paleozoic in the more recent version of COPSE (Lenton and others, 2016). Therefore, the COPSE model is parameterized in such a way as to directly drive a rise in atmospheric oxygen levels with the emergence of land plants, and thus does not provide truly independent support for the link between land plant evolution and global oxygenation.

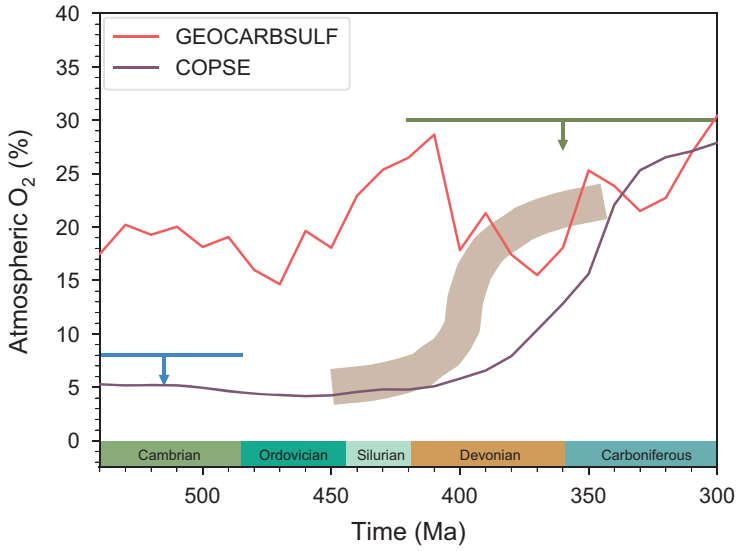

Fig. 1. O_2 evolution patterns through the Paleozoic. The red curve represents the O_2 prediction from the GEOCARBSULF model (Royer and others, 2014). The purple curve represents the O_2 prediction from the baseline COPSE model (Bergman and others, 2004). The blue line shows the approximate maximum atmospheric O_2 level based on water column redox data (Canfield, 1998; Sperling and others, 2015). The green line is the approximate O_2 maximum, based on burning experiments and wildfire feedbacks (Watson and others, 1978; Belcher and McElwain, 2008; Glasspool and others, 2015), but geochemical mass balance studies suggest pO_2 levels as high as 35% may be permissible (Wildman and others, 2004). The brown shaded area represents the hypothesized trend of atmospheric O_2 evolution based on Mo isotopes (Dahl and others, 2010) and cerium anomaly records (Wallace and others, 2017).

Here, we revisit GEOCARBSULF to explore if this model can generate estimates of pO_2 consistent with the premise that land plants reshaped our atmosphere. Specifically, we test whether atmospheric O_2 can be maintained at relatively low levels in the early Paleozoic, and then rise over the latter half of the Paleozoic in GEOCARBSULF. We address this question by investigating the sources and sinks of O_2, as shown in equation (3). First, we conduct sensitivity analyses on the weathering and degassing of the carbon and sulfur reservoirs, which directly influence the O_2 sinks, but also determine the O_2 sources indirectly, through their control on the burial rate of organic carbon and pyrite. Second, we investigate the effect on O_2 levels by a single term — the $\delta^{13}C$ value of buried carbonate through time, which directly reflects the burial of organic carbon and in turn regulates the rates of O_2 release. In addition, we use a more reasonable value of the initial sulfate proportion in the crust and perform sensitivity analyses on the $\delta^{13}C$ value of buried carbonate using this updated value. Building from this work we argue that GEOCARBSULF can produce low Paleozoic O_2 levels by only varying the $\delta^{13}C$ values within the uncertainties of the geological record. In other words, the variation of $\delta^{13}C$ values of carbonate can play a big role in controlling the model output. More accurate predictions of GEOCARBSULF will come from an improved C isotope record.

A BRIEF INTRODUCTION TO GEOCARBSULF

GEOCARBSULF was constructed based upon a series of seminal studies on global carbon and sulfur cycling. Numerical models for reconstructing the mass of oxidized and reduced carbon and sulfur through the Phanerozoic build heavily upon the work of Garrels and Lerman (1981, 1984), which outlined the central tenets in global

isotope mass balance modeling. Berner (1987) made a major modification when he put forward the idea of "rapid recycling" to provide strong negative feedback on O_2 fluctuations and predicted atmospheric O_2 evolution through the Phanerozoic. In rapid recycling, the mass of each sedimentary reservoir is divided into young (rapidly weathering) and old (slowly weathering) components. All newly buried carbon and sulfur go to the young reservoirs. In this way, whenever a substantial amount of organic carbon or pyrite is quickly buried (leading to rapid O_2 release), there is subsequent enhancing of the weathering rate of the young organic carbon and pyrite reservoirs (leading to rapid O_2 consumption), which will mitigate the fluctuation of O_2 levels. To provide a stronger negative feedback, Berner and others (2000) and Berner (2001) incorporated O_2-dependent carbon and sulfur isotope fractionation into the model. In 2006, Berner combined GEOCARB III (a classic model to reconstruct the CO_2 levels in the past, largely developed by Berner) and the O_2 model into a single model called GEOCARBSULF, which could simultaneously calculate the evolution of CO_2 and O_2 through the Phanerozoic (Berner, 2006b). In the following years, GEOCARBSULF was continuously updated and refined (for example, with the inclusion of the weathering of volcanic rocks and reconsideration of the fractionation of carbon isotopes) (Berner, 2006a; Berner, 2009) and the most recent version is described by Royer and others (2014).

An overview of the geochemical cycles of carbon, sulfur and oxygen in GEOCARBSULF is presented in figure 2. The full equations and parameters of GEOCARBSULF are described in detail in the Appendix. Below we list the key equations (with parameters defined in fig. 2 and the Appendix) in GEOCARBSULF that are used to calculate the fluxes related to O_2 evolution.

$$F_{wgy} = f_A \cdot f_R \cdot \mathrm{k_{wgy}} \cdot G_y(t) \tag{4}$$

$$F_{wga} = f_R \cdot F_{wga\_}0 \tag{5}$$

$$F_{wcy} = f_A \cdot f_D \cdot f_L \cdot f_E \cdot f_{Bb\_ca} \cdot k_{wcy} \cdot C_y(t) \tag{6}$$

$$F_{wca} = f_A \cdot f_D \cdot f_L \cdot f_E \cdot f_{Bb\_ca} \cdot F_{wca\_}0 \tag{7}$$

$$F_{wpy} = f_A \cdot f_R \cdot \mathrm{k_{wpy}} \cdot \mathrm{P}_y(t) \tag{8}$$

$$F_{wpa} = f_R \cdot F_{wpa\_}0 \tag{9}$$

$$F_{wsy} = f_A \cdot f_D \cdot \mathrm{k_{wsy}} \cdot S_y(t) \tag{10}$$

$$F_{wsa} = f_A \cdot f_D \cdot F_{wsa\_}0 \tag{11}$$

$$F_{mg} = f_{SR} \cdot F_{mg\_}0 \tag{12}$$

$$F_{mc} = f_{SR} \cdot f_C \cdot F_{mc\_}0 \tag{13}$$

$$F_{mp} = f_{SR} \cdot F_{mp\_}0 \tag{14}$$

$$F_{ms} = f_{SR} \cdot F_{ms\_}0 \tag{15}$$

$$F_{bg} = \frac{1}{\Delta^{13}C} \times [(\delta^{13}C - dlcy) \cdot F_{wcy} + (\delta^{13}C - dlca) * F_{wca} + (\delta^{13}C - dlgy) * F_{wgy} + (\delta^{13}C - dlga) * F_{wga} + (\delta^{13}C - dlca) * F_{mc} + (\delta^{13}C - dlga) * F_{mg}] \tag{16}$$

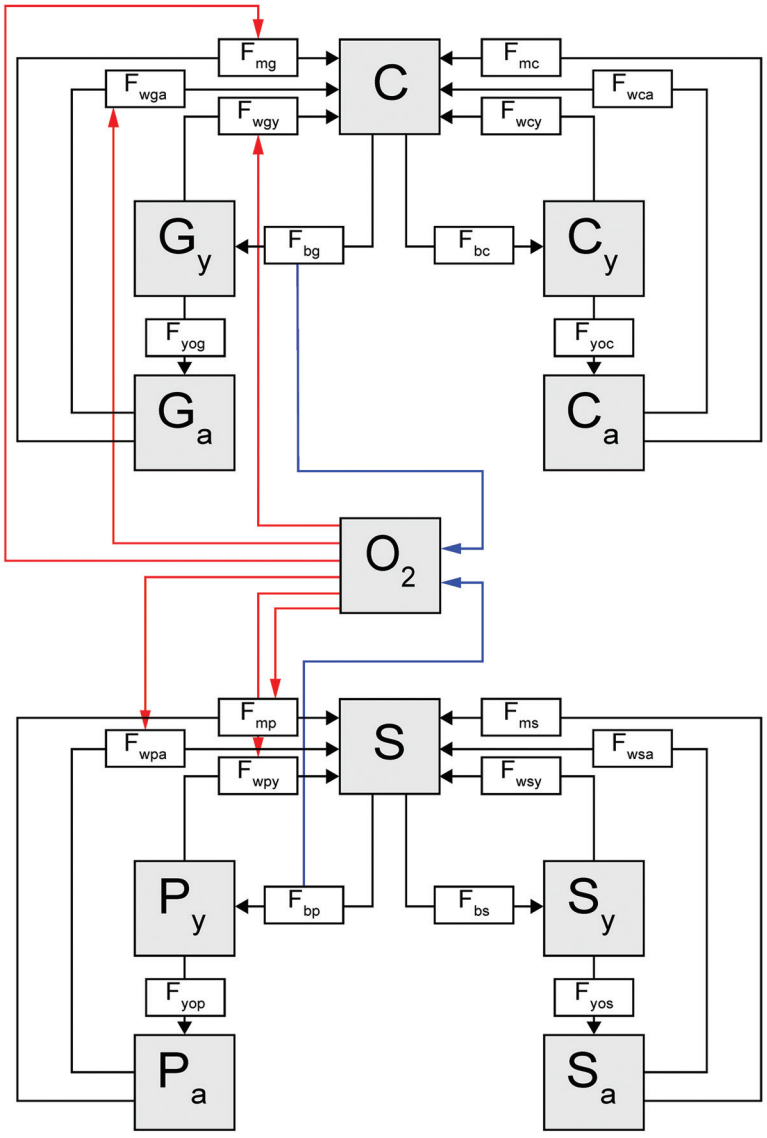

Fig. 2. Long-term carbon, sulfur, and oxygen cycles in GEOCARBSULF. Carbon cycle consists of fluxes between carbon in the surficial system including atmosphere, ocean, biosphere and soil (**C**), young organic carbon ($\mathbf{G_y}$), old organic carbon ($\mathbf{G_a}$), young carbonate ($\mathbf{C_y}$) and old carbonate ($\mathbf{C_a}$). Specifically, these fluxes are organic carbon burial ($\mathbf{F_{bg}}$), oxidative weathering of young organic carbon ($\mathbf{F_{wgy}}$) and old organic carbon ($\mathbf{F_{wga}}$), degassing of organic carbon from volcanism, metamorphism and diagenesis ($\mathbf{F_{mg}}$), organic carbon transfer from young to old reservoirs ($\mathbf{F_{yog}}$), carbonate burial ($\mathbf{F_{bc}}$), weathering of young carbonate ($\mathbf{F_{wcy}}$) and old carbonate ($\mathbf{F_{wca}}$), degassing of carbonate from volcanism, metamorphism and diagenesis ($\mathbf{F_{mc}}$), and carbonate transfer from young to old reservoirs ($\mathbf{F_{yoc}}$). Sulfur cycle consists of fluxes between sulfur in the surficial system including atmosphere, ocean, biosphere and soil (**S**), young pyrite sulfur ($\mathbf{P_y}$), old pyrite sulfur ($\mathbf{P_a}$), young gypsum sulfur ($\mathbf{S_y}$) and old gypsum sulfur ($\mathbf{S_a}$). Specifically, these fluxes include pyrite burial ($\mathbf{F_{bp}}$), oxidative weathering of young pyrite ($\mathbf{F_{wpy}}$) and old pyrite ($\mathbf{F_{wpa}}$), degassing of pyrite from volcanism, metamorphism and diagenesis ($\mathbf{F_{mp}}$), pyrite transfer from young to old reservoirs ($\mathbf{F_{yop}}$), gypsum burial ($\mathbf{F_{bs}}$), weathering of young gypsum ($\mathbf{F_{wsy}}$) and old gypsum ($\mathbf{F_{wsa}}$), degassing of gypsum from volcanism, metamorphism and diagenesis ($\mathbf{F_{ms}}$), and gypsum transfer from young to old reservoirs ($\mathbf{F_{yos}}$). As shown in equation (18), the sources of atmospheric O_2 are $\mathbf{F_{bg}}$ and $\mathbf{F_{bp}}$ (represented by the blue arrows). The sinks are $\mathbf{F_{wgy}}$, $\mathbf{F_{wga}}$, $\mathbf{F_{mg}}$, $\mathbf{F_{wpy}}$, $\mathbf{F_{wpa}}$ and $\mathbf{F_{mp}}$ (represented by the red arrows).

$$F_{bp} = \frac{1}{\Delta^{34}S} \times [(\delta^{34}S - dlsy) \cdot F_{wsy} + (\delta^{34}S - dlsa) * F_{wsa} + (\delta^{34}S - dlpy) * F_{wpy} + (\delta^{34}S - dlpa) * F_{wpa} + (\delta^{34}S - dlsa) * F_{ms} + (\delta^{34}S - dlpa) * F_{mp}] \quad (17)$$

$$\frac{d[O_2]}{dt} = F_{bg} - F_{wgy} - F_{wga} - F_{mg} + \left(\frac{15}{8}\right)(F_{bp} - F_{wpy} - F_{wpa} - F_{mp}) \quad (18)$$

Using the "rapid recycling" concept, the weatherable crust is divided into young reservoirs (Gy, Cy, Py, Sy) and old reservoirs (Ga, Ca, Pa, Sa). The isotope mass balance technique is given in equations (16) and (17). In addition to the terms defined above (and in the caption of fig. 2), f_A is land area at time (t) relative to the present a day; f_D is global river runoff at time (t) relative to the present-day in the absence of changing CO_2 and solar luminosity; f_L is land area covered by carbonates at time (t) relative to the present-day; f_R is effect of relief on chemical weathering at time (t) relative to the present-day; f_{SR} is seafloor creation rate at time (t) relative to the present-day; f_E is effect of plants on weathering rate at time (t) relative to the present-day; f_{Bb_ca} is the combined effect of changes to temperature and CO_2 on carbonate weathering; k_{wgy} is rate of mass dependence for young organic carbon weathering; k_{wcy} is rate of mass dependence for young carbonate weathering; k_{wpy} is rate of mass dependence for young pyrite sulfur weathering; k_{wsy} is rate of mass dependence for young sulfate sulfur weathering; F_{wga_0} is the carbon flux from weathering of old sedimentary organic matter at present-day; F_{wca_0} is the carbon flux from weathering of old carbonates at present-day; F_{wpa_0} is the sulfur flux from weathering of old pyrite at present-day; F_{wsa_0} is the sulfur flux from weathering of old sulfate at present-day; F_{mg_0} is the carbon degassing flux of organic carbon at present-day; F_{mc_0} is the carbon degassing flux of carbonates at present-day; F_{mp_0} is the sulfur degassing flux of pyrite at present-day; F_{ms_0} is the sulfur degassing flux of sulfate at present-day; $\Delta^{13}C$ is the carbon isotope fractionation between carbonate and organic carbon; $\delta^{13}C$ is the isotope value of carbonate carbon; dlgy, dlga, dlcy and dlca are the $\delta^{13}C$ values of young organic carbon, old organic carbon, young carbonate carbon and old carbonate carbon respectively; $\Delta^{34}S$ is the sulfur isotope fractionation between gypsum and pyrite; $\delta^{34}S$ is the isotope values of gypsum sulfur; dlpy, dlpa, dlsy and dlsa are the $\delta^{34}S$ values of young pyrite sulfur, old pyrite sulfur, young gypsum sulfur and old gypsum sulfur respectively.

MODIFICATION TO GEOCARBSULF

We modified the GEOCARBSULF version presented by Royer and others (2014), which is largely identical to the initial versions of GEOCARBSULF (Berner, 2006b; Berner, 2009). In GEOCARBSULF, carbon and sulfur isotope fractionation ($\Delta^{13}C$ and $\Delta^{34}S$) is dependent on O_2 levels, which can provide a negative feedback to any fluctuations of O_2 and thus helps the model to avoid unrealistic atmospheric O_2 levels throughout the Phanerozoic. Their relationship can be formulated as follows:

$$\Delta^{13}C = \Delta^{13}C\_0 + [J \cdot (RO_2 - 1)] \quad (19)$$

$$\Delta^{34}S = \Delta^{34}S\_0 \times RO_2^n \quad (20)$$

Where $\Delta^{13}C\_0$ represents the carbon isotopic fractionation between carbonate and organic matter at present-day; J is an adjustable curve fit parameter; RO_2 is the mass of oxygen in the atmosphere in the past relative to the present-day; $\Delta^{34}S\_0$ represents the sulfur isotopic fractionation between gypsum and pyrite at present-day; n is an adjustable fit parameter. Unlike the relationship between O_2 and the carbon isotope fractionation factor ($\Delta^{13}C$), which is based on lab experiments (Berner and

others, 2000; Beerling and others, 2002), the O_2 dependency of $\Delta^{34}S$ is not well constrained (Canfield, 2001; Johnston, 2011; Sim and others, 2011) and the relationship used in GEOCARBSULF is likely overly simplified.

To quantify $\Delta^{34}S$ through time, Wu and others (2010) adopted two methods: an arithmetic difference method ($\Delta^{34}S = \delta^{34}S_{sw} - \delta^{34}S_{py}$) which is totally based on geological empirical records, and an independent method that calls upon $\Delta^{33}S$ and sulfur cycle models. These two methods yield similar results (particularly before the Permian) and prove the robustness of using the empirical records to determine $\Delta^{34}S$. Although those geological records can only represent a small fraction of what was deposited, they do construct the current best available $\Delta^{34}S$ curve. Therefore, in our revised model calculations, we used an empirically based record of $\Delta^{34}S$ (and assign 4‰ as the 2SD), which eliminates the strong O_2 feedback in the sulfur cycle. We also updated GEOCARBSULF by replacing the old $\delta^{13}C$ curve with the new 10 million years average curve (Veizer and others, 1999; Grossman and others, 2008; Saltzman and Thomas, 2012). Similar to Royer and others (2014), we used a Monte Carlo approach (10000 resampling) to quantify the errors of the model outputs. During each resample, GEOCARBSULF can fail at a specific time step for several reasons: 1) Any carbon or sulfur flux goes negative; 2) Calculated CO_2 is less than 150 ppm or bigger than 50000 ppm; 3) Calculated CO_2 or O_2 at 0 Ma deviates from their measured values (CO_2 is not in the 200–300 ppm range and O_2 is not in the 19–23% range) (Royer and others, 2014). Following the above two updates, we ran GEOCARBSULF with a starting atmospheric O_2 level of 1 percent and 5 percent respectively at 570 Ma. We also ran GEOCARBSULF with the updated $\delta^{13}C$ curve but kept the old $\Delta^{34}S$ formulation. Compared with the model run using the old $\Delta^{34}S$ formulation (fig. 3A), using the updated $\Delta^{34}S$ did not help to lower O_2 levels in the early Paleozoic (fig. 3B), but it did serve to remove an unrealistic negative feedback from the model.

The key tenet of our new method (sensitivity tests) is that we are able to input the desired model output (that is, O_2 evolution) and observe the underlying parameter changes required for the model to generate such an output. This is a modification of the traditional use of GEOCARBSULF where one predicts O_2 evolution from carbon and sulfur fluxes and isotope records. One set of underlying parameters that can be explored using this new method is the weathering and degassing fluxes of carbonates, organic carbon, sulfate and pyrite, which can affect the O_2 sink, as well as the O_2 source via isotope mass balance (equations 16 and 17). There are large uncertainties for these parameters in the current version of GEOCARBSULF. For example, the total land area that experienced extensive weathering, and the global runoff through time, are not well constrained (Royer and others, 2014). In addition, the oxygen dependency of the weathering rate of organic carbon and pyrite is debated (for example, Lasaga and Ohmoto, 2002; Bolton and others, 2006). The volcanic degassing rate, directly linked to degassing fluxes of carbon and sulfur, is likewise under continuous revision (for example, Berner, 2004; Van Der Meer and others, 2014; McKenzie and others, 2016). Another underlying parameter that has large uncertainties is the $\delta^{13}C$ of marine dissolved inorganic carbon (DIC), which is derived from buried carbonate and influences the calculated organic carbon burial rate — a key O_2 source. The record of burial carbonate $\delta^{13}C$ before the Mid-Jurassic is predominantly from measurements of platform carbonates, which exhibit greater spatial heterogeneity in $\delta^{13}C$ values than the Mid-Jurassic to Cenozoic measurements of pelagic carbonates (Panchuk and others, 2006; Saltzman and Thomas, 2012). Lastly, the initial reservoir sizes of sulfate and pyrite in the crust, which will shape Paleozoic redox conditions, are poorly constrained.

Here, we use the new method to test whether GEOCARBSULF can maintain a low atmospheric O_2 level in the early Paleozoic given available empirical constraints. To do

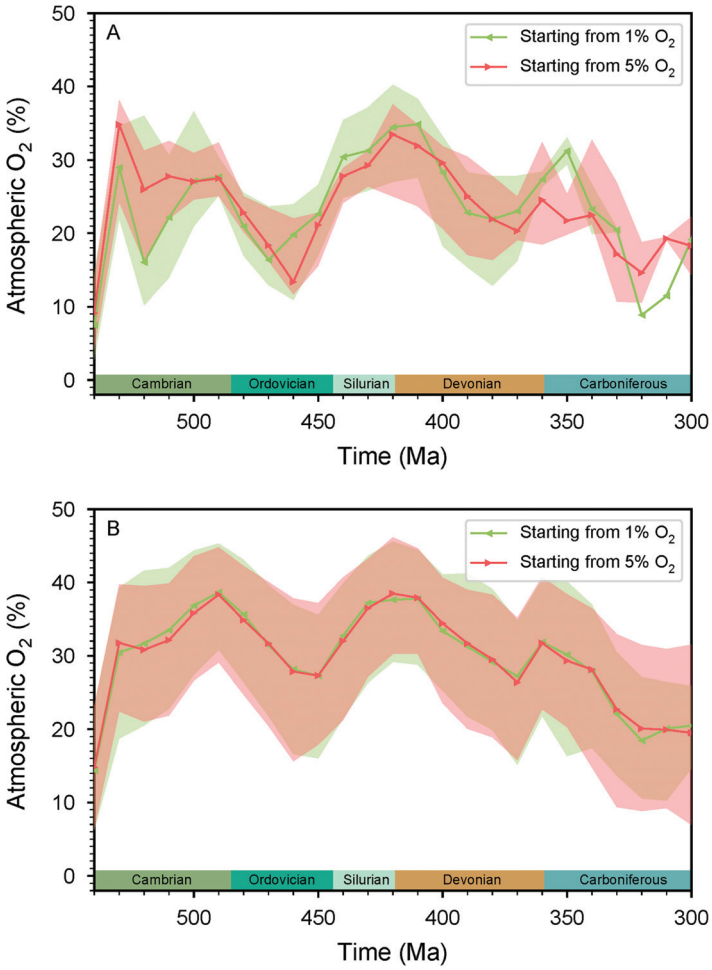

Fig. 3. Predicted O_2 evolution from the GEOCARBSULF model with an initial O_2 level of 1% and 5%. (A) $\Delta^{34}S$ is derived from the old formulation (O_2 dependency) in GEOCARBSULF. (B) $\Delta^{34}S$ is derived from the geological records (Wu and others, 2010). The green line represents the predicted average O_2 level staring from 1% at 570 Ma and the red line represents the predicted average O_2 level staring from 5% at 570 Ma. The shaded area represents the average value ± 1SD.

this, we first constructed four example pO_2 evolution scenarios through the Paleozoic (fig. 4), which are based on paleo-proxy records and previous model studies (fig. 1) and these will be used as an input to our new methods in the following sections. We used scenarios that cover a wide spectrum of delayed O_2 evolution patterns and thus can be used to test the potential for predicting these oxygenation histories using GEOCARBSULF.

Sensitivity tests of the weathering and degassing fluxes of carbon and sulfur on O_2 levels

We applied our new method to investigate the sensitivity of O_2 levels to the weathering and degassing fluxes of different rock reservoirs, namely carbonate weathering (F_{wcy} and F_{wca}), organic carbon weathering (F_{wgy} and F_{wga}), carbonate degassing (F_{mc}), organic carbon degassing (F_{mg}), sulfate weathering (F_{wsy} and F_{wsa}), sulfate

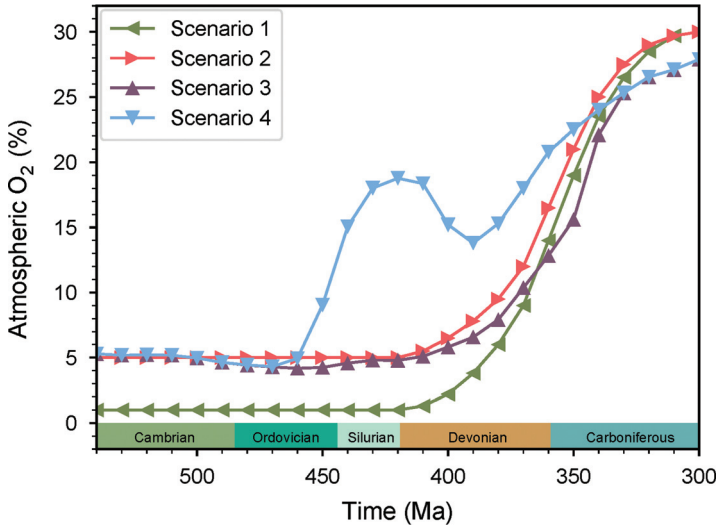

Fig. 4. Atmospheric O_2 evolution scenarios through the Paleozoic constructed in this study. Scenario 1 and 2 try to simulate the O_2 level predicted by the cerium anomaly (Wallace and others, 2017). They keep O_2 at a low level (1% and 5% respectively) from the Early Cambrian to the Late Silurian and then force O_2 to rise to ~30% by the Late Carboniferous. Scenario 3 is atmospheric O_2 evolution after the baseline COPSE model (Bergman and others, 2004). Scenario 4 is a combination of atmospheric O_2 prediction after the baseline COPSE model and the updated COPSE model which integrates early plant colonization, biotic effects on silicate weathering and 25% increase in P weathering (Lenton and others, 2016).

degassing (F_{ms}), pyrite weathering (F_{wpy} and F_{wpa}), and pyrite degassing (F_{mp}). We used a general-purpose optimization routine (L-BFGS-B in R language) to solve all the weathering and degassing fluxes of carbon and sulfur. Specifically, we multiply these fluxes each by a scaling factor, aiming to evaluate the relative importance of these fluxes in controlling pO_2. The modified equations are as follows (_S means scaling):

$$F_{wgy\_}S = S_{wg} \cdot f_A \cdot f_R \cdot \mathrm{k_{wgy}} \cdot G_y(t) \tag{21}$$

$$F_{wga\_}S = S_{wg} \cdot f_R \cdot F_{wga\_}0 \tag{22}$$

$$F_{wcy\_}S = S_{wc} \cdot f_A \cdot f_D \cdot f_L \cdot f_E \cdot f_{Bb\_ca} \cdot k_{wcy} \cdot C_y(t) \tag{23}$$

$$F_{wca\_}S = S_{wc} \cdot f_A \cdot f_D \cdot f_L \cdot f_E \cdot f_{Bb\_ca} \cdot F_{wca\_}0 \tag{24}$$

$$F_{wpy\_}S = S_{wp} \cdot f_A \cdot f_R \cdot \mathrm{k_{wpy}} \cdot P_y(t) \tag{25}$$

$$F_{wpa\_}S = S_{wp} \cdot f_R \cdot F_{wpa\_}0 \tag{26}$$

$$F_{wsy\_}S = S_{ws} \cdot f_A \cdot f_D \cdot \mathrm{k_{wsy}} \cdot S_y(t) \tag{27}$$

$$F_{wsa\_}S = S_{ws} \cdot f_A \cdot f_D \cdot F_{wsa\_}0 \tag{28}$$

$$F_{mg\_}S = S_{mg} \cdot f_{SR} \cdot F_{mg\_}0 \tag{29}$$

$$F_{mc\_}S = S_{mc} \cdot f_{SR} \cdot f_C \cdot F_{mc\_}0 \tag{30}$$

$$F_{mp\_}S = S_{mp} \cdot f_{SR} \cdot F_{mp\_}0 \tag{31}$$

$$F_{ms\_}S = S_{ms} \cdot f_{SR} \cdot F_{ms\_}0 \tag{32}$$

$$F_{bg\_}S = \frac{1}{\Delta^{13}C} \times [(\delta^{13}C - dlcy) \cdot F_{wcy\_}S + (\delta^{13}C - dlca) * F_{wca\_}S + (\delta^{13}C - dlgy) * F_{wgy\_}S + (\delta^{13}C - dlga) * F_{wga\_}S + (\delta^{13}C - dlca) * F_{mc\_}S + (\delta^{13}C - dlga) * F_{mg\_}S] \quad (33)$$

$$F_{bp\_}S = \frac{1}{\Delta^{34}S} \times [(\delta^{34}S - dlsy) \cdot F_{wsy\_}S + (\delta^{34}S - dlsa) * F_{wsa\_}S + (\delta^{34}S - dlpy) * F_{wpy\_}S + (\delta^{34}S - dlpa) * F_{wpa\_}S + (\delta^{34}S - dlsa) * F_{ms\_}S + (\delta^{34}S - dlpa) * F_{mp\_}S] \quad (34)$$

$$\frac{d[O_2]}{dt} = F_{bg\_}S - F_{wgy\_}S - F_{wga\_}S - F_{mg\_}S + \left(\frac{15}{8}\right)(F_{bp\_}S - F_{wpy\_}S - F_{wpa\_}S - F_{mp\_}S) \quad (35)$$

The method searches for the optimized value for each scaling factor (as close as possible to 1, meaning the new flux is as close as possible to the original flux) needed to match a predicted O_2 at each time step. Using equation (21) to (35), we solve $F_{ms\_}S$ in terms of $F_{wgy\_}S$, $F_{wga\_}S$, $F_{wcy\_}S$, $F_{wca\_}S$, $F_{wpy\_}S$, $F_{wpa\_}S$, $F_{wsy\_}S$, $F_{wsa\_}S$, $F_{mg\_}S$, $F_{mc\_}S$, $F_{mp\_}S$ and $d[O_2]/dt$. Afterwards, to achieve the optimization goal, we use L-BFGS-B to minimize the following expression:

$$\left|\frac{F_{wgy\_}S + F_{wga\_}S - F_{wgy} - F_{wga}}{F_{wgy} + F_{wga}}\right| + \left|\frac{F_{wcy\_}S + F_{wca\_}S - F_{wcy} - F_{wca}}{F_{wcy} + F_{wca}}\right| + \left|\frac{F_{wpy\_}S + F_{wpa\_}S - F_{wpy} - F_{wpa}}{F_{wpy} + F_{wpa}}\right| + \left|\frac{F_{wsy\_}S + F_{wsa\_}S - F_{wsy} - F_{wsa}}{F_{wsy} + F_{wsa}}\right| + \left|\frac{F_{mg\_}S - F_{mg}}{F_{mg}}\right| + \left|\frac{F_{mc\_}S - F_{mc}}{F_{mc}}\right| + \left|\frac{F_{mp\_}S - F_{mp}}{F_{mp}}\right| + \left|\frac{F_{ms\_}S - F_{ms}}{F_{ms}}\right| \quad (36)$$

We assign a lower bound of 0 to the seven scaling factors (carbonate weathering, organic carbon weathering, carbonate degassing, organic carbon degassing, sulfate weathering, pyrite weathering and pyrite degassing) and assign no bound to the scaling factor of sulfate degassing (since this scaling factor is solved from the other seven scaling factors). The model runs from 570 to 300 Ma but fails at various time steps for different scenarios. In addition, some scaling factors are required to fluctuate significantly within a geologically short time interval, which is physically implausible. For example, for the carbonate weathering scaling factor (fig. 5B), extremely large fluctuations (a drop from 1 to 0 in 20 million years during the Ordovician for Scenario 3 and 4) are required.

Sensitivity tests of carbonate $\delta^{13}C$ on O_2 levels

We argue that the most poorly constrained, yet impactful, parameter for GEOCARBSULF is the carbonate $\delta^{13}C$ input to the model as it tightly controls the burial rate of organic carbon. Due to the complexity surrounding the empirical carbonate $\delta^{13}C$ records, the $\delta^{13}C$ of buried carbonate in the Paleozoic used in GEOCARBSULF may not be the true average $\delta^{13}C$ of the ocean (for example, Saltzman and Thomas, 2012). And as demonstrated in Royer and others (2014) and Mills and others (2016), the atmospheric O_2 predicted by isotope mass balance is highly sensitive to assumed carbonate $\delta^{13}C$. Assuming all the weathering and degassing fluxes of carbon and sulfur are the same as in the original GEOCARBSULF (that is, all

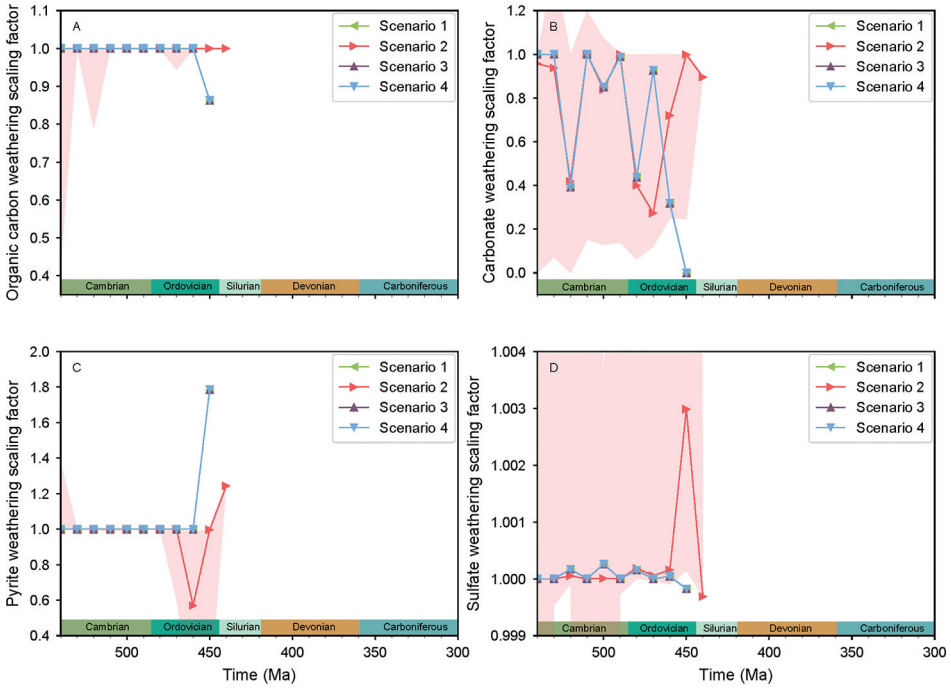

Fig. 5. The scaling factors for various weathering fluxes required to reproduce different O_2 scenarios. (A) Scaling factor for the organic carbon weathering rate. (B) Scaling factor for the carbonate weathering rate. (C) Scaling factor for the pyrite weathering rate. (D) Scaling factor for the sulfate weathering rate. The shaded pink area represents the average value ± 2SD for Scenario 2. The error range for other scenarios is similar to that of Scenario 2. Different scenarios are described in figure 4.

scaling factors are 1), it is straightforward to apply the new method to solve for carbonate $\delta^{13}C$, for different O_2 scenarios. Since we only have 1 unknown parameter (carbonate $\delta^{13}C$), we directly solve for this parameter and its solution is as follows:

$$\delta^{13}C = \frac{F_{bg} \cdot \Delta^{13}C + F_{wcy} \cdot \mathrm{dlcy} + F_{wca} \cdot \mathrm{dlca} + F_{wgy} \cdot \mathrm{dlgy} + F_{wga} \cdot \mathrm{dlga} + F_{mc} \cdot \mathrm{dlca} + F_{mg} \cdot \mathrm{dlga}}{F_{wcy} + F_{wca} + F_{wgy} + F_{wga} + F_{mc} + F_{mg}} \quad (37)$$

As shown in figure 6, the carbonate $\delta^{13}C$ required to fit each O_2 scenario is consistently within the range of $\delta^{13}C$ records through the Paleozoic, and is almost always within 2SD of the long term running average. The overall evolving trends of the required $\delta^{13}C$ across all scenarios and the $\delta^{13}C$ record are similar, and the CO_2 predicted is similar to that from the original GEOCARBSULF model (fig. 7). In all scenarios, the organic carbon burial rate increased through the Devonian (fig. 8A) and the pyrite burial rate decreased through the Paleozoic (fig. 8B).

Instead of calculating $\Delta^{13}C$ based on its relationship with O_2 levels, we can also derive $\Delta^{13}C$ through time from the geologic records (fig. 9A, Hayes and others, 1999), as we did for $\Delta^{34}S$. We note that the compilation of Hayes and others (1999) may not represent the true global average $\Delta^{13}C$ because the $\delta^{13}C$ of organic carbon used to calculate $\Delta^{13}C$ is based solely on marine organic matter. Despite this, the required

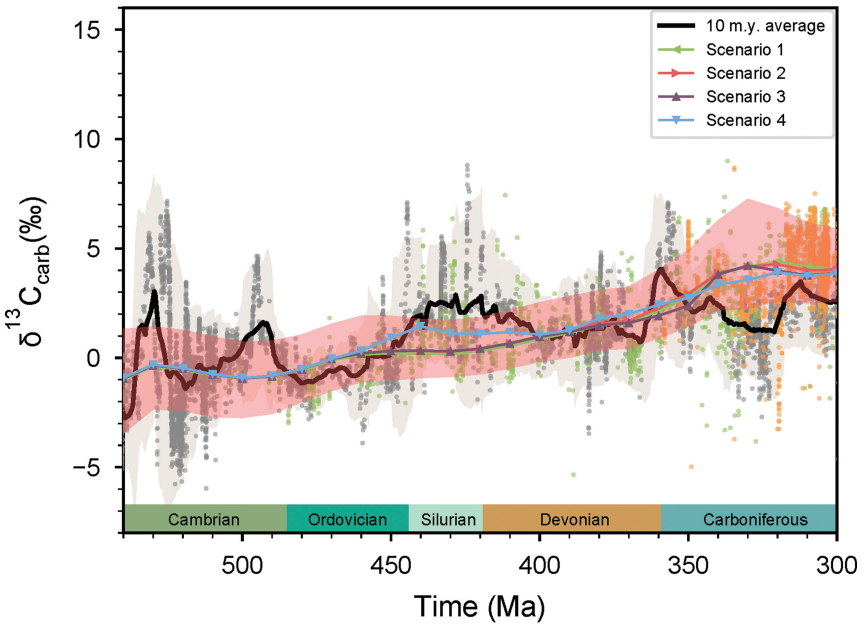

Fig. 6. Carbonate $\delta^{13}C$ required to reproduce the four oxygen scenarios through the Paleozoic, and how they correlate with the geologic record. The gray dots are the carbonate $\delta^{13}C$ values compiled from Saltzman and Thomas (2012). The green dots are the $\delta^{13}C$ values of brachiopod shells from Veizer (1999). The orange dots are the $\delta^{13}C$ values of brachiopod shells compiled by Grossman and others (2008). The black line represents the moving average (10 Myrs) of all the carbonate $\delta^{13}C$ records. The brown area represents the average value ± 2SD. The shaded pink area represents the average value ± 2SD for Scenario 2. The error range for other scenarios is similar to that of Scenario 2. Different scenarios are described in figure 4.

carbonate $\delta^{13}C$ values still fall into the range of the $\delta^{13}C$ record after this update (fig. 9B).

Besides carbonate $\delta^{13}C$, the initial sulfate proportion within the upper continental crust (50% of the total sulfur) at 570 Ma assumed in the original GEOCARBSULF is considered unlikely based on several recent f_{py} estimates (for example, Canfield and Farquhar, 2009; Halevy and others, 2012) which argue for limited sulfate burial in the Precambrian and Early Cambrian. Therefore, as an initial attempt, we reduced the initial sulfate proportion in the crust from 50 percent to 20 percent, which is in qualitative agreement with the work of Canfield and Farquhar (2009). To maintain a realistic $\delta^{34}S$ value of the sulfate reservoirs after this proportion change, the $\delta^{34}S$ values of initial young and old pyrite in the original GEOCARBSULF are also adjusted (from -10‰ to 0‰). This change is not unreasonable, as the $\delta^{34}S$ of buried sedimentary pyrite was 5.7 permil at 570 Ma and was even higher than 5.7 permil in the Precambrian (Wu and others, 2010). Therefore, assigning 0 permil to the initial sedimentary pyrite is conservative. After these modifications, the required carbonate $\delta^{13}C$ is more enriched at each time step (fig. 10 vs fig. 6) but still fits reasonably well with the isotope records. The CO_2 predictions are again similar to the original GEOARBSULF (fig. 11).

DISCUSSION

Our sensitivity tests demonstrate that it is impossible to maintain a low atmospheric O_2 in the early Paleozoic followed by an O_2 rise to ~ 30 percent by the Late Carboniferous through varying only the weathering and degassing fluxes of different

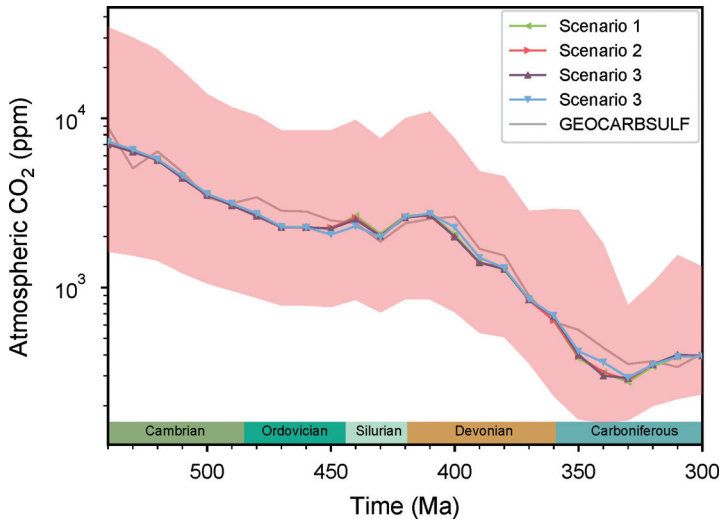

Fig. 7. Atmospheric CO_2 predicted in the sensitivity tests of carbonate $\delta^{13}C$ for different scenarios, compared with the CO_2 predicted from the original GEOCARBSULF (Royer and others, 2014). Different scenarios are described in figure 4.

rock reservoirs in GEOCARBSULF. Even over the short time interval where the model ran successfully and maintained consistent O_2 levels, some weathering and degassing rate variations were extreme, indicating inefficiency of these parameters in controlling atmospheric O_2. While these results confirm that inorganic weathering and degassing fluxes can alter the predictions drawn from carbon isotope mass balance (Shields and Mills, 2017), they also suggest that the dominant influence on O_2 variability over most of the Phanerozoic was not the weathering rates of organic carbon and pyrite but their burial rates (Berner, 2006b).

By removing the extreme negative feedback from the sulfur system and changing the input carbonate $\delta^{13}C$ within the geological data range, we can maintain a low O_2 level in GEOCARBSULF before the Devonian (or before the Silurian in the case of Scenario 4 — see fig. 4). This model output is in great contrast with that of Royer and others (2014), which could not produce low O_2 levels in the early Paleozoic. Compared with figure 3B, which also could not maintain a low O_2 level even after updating the $\delta^{13}C$ and $\Delta^{34}S$, our model outputs indicate that uncertainity over the variations in marine $\delta^{13}C$ is the biggest hurdle in predicting O_2. Our method also argues for a relatively constant organic carbon burial rate through the Ordovician and Silurian, and a continuous increase of the organic carbon burial rate through the Devonian (fig. 8A), which correlates with the diversification of vascular plants. Our predicted $\delta^{13}C$ is generally less variable than the observed record through this time (figs. 6 and 10). However, the empirical $\delta^{13}C$ of old platform carbonates, similar to modern shallow water carbonates, were likely influenced by many factors such as: diagenetic processes, mineralogical variability, vital effects caused by calcifying organisms, local water mass restriction, and carbon cycle perturbations (Mii and others, 1999; Veizer and others, 1999; Panchuk and others, 2006; Brand and others, 2009; Saltzman and Thomas, 2012). For example, the $\delta^{13}C$ of brachiopods exhibit substantial regional heterogeneity, with high values in the Russian Platform, low values in western North America, and intermediate values in the midcontinent (Grossman and others, 2008). Given this variability, the exact global curve of the carbonate $\delta^{13}C$ through the Paleozoic is poorly

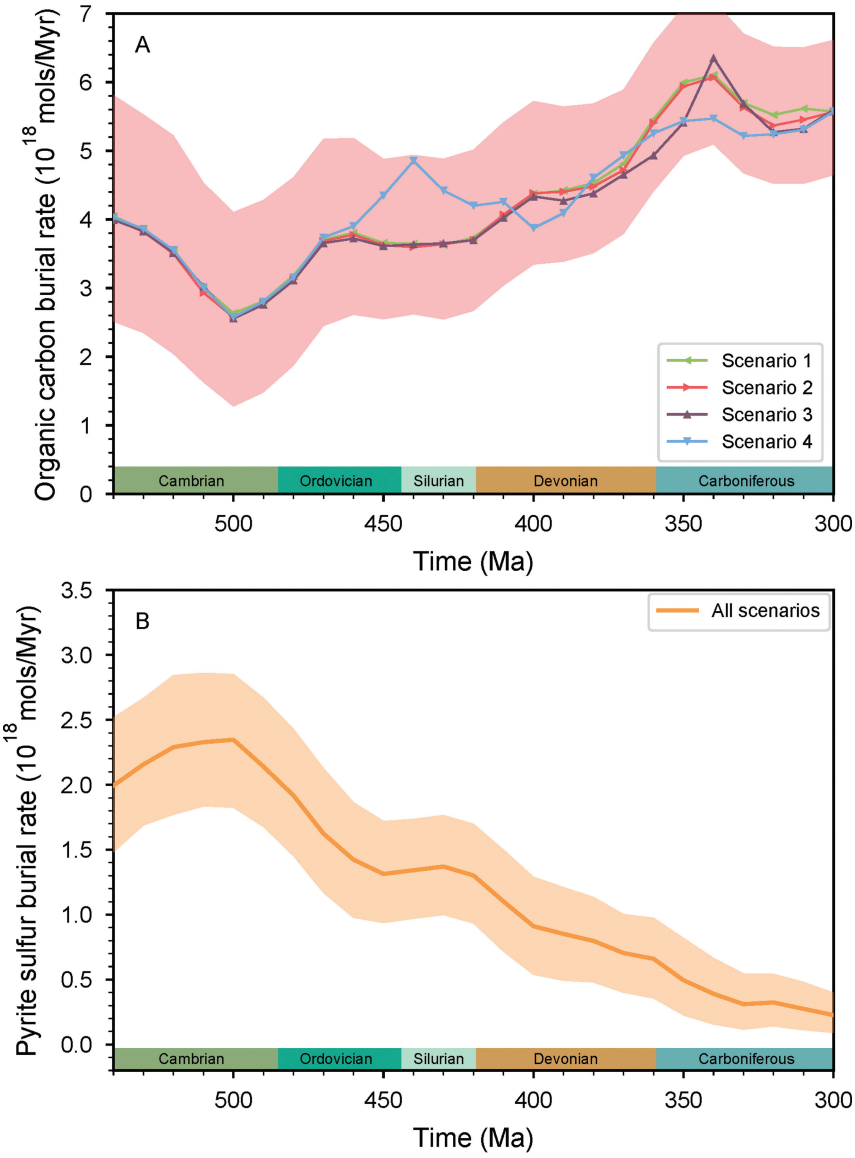

Fig. 8. Organic carbon and pyrite sulfur burial rates predicted in the sensitivity tests of carbonate $\delta^{13}C$ for different scenarios. (A) Organic carbon (C) burial rate. (B) Pyrite sulfur (S) burial rate. Notice that the pyrite burial rates for different scenarios are the same. Different scenarios are described in figure 4.

known. Our modeling approach serves as an indirect way to inspect the global average carbonate $\delta^{13}C$ and bears significance for promoting further research on this issue.

There are uncertainties in many of the parameters in GEOCARBSULF and it is possible that some key processes are entirely absent from the model (Royer and others, 2014). Also, as a critical O_2 source, we note that the organic carbon burial rate calculated using the isotope mass balance method needs to be further examined and compared with geological records. But we have shown here that high atmospheric oxygen in the Paleozoic is not a reliable output from GEOCARBSULF, and low levels of

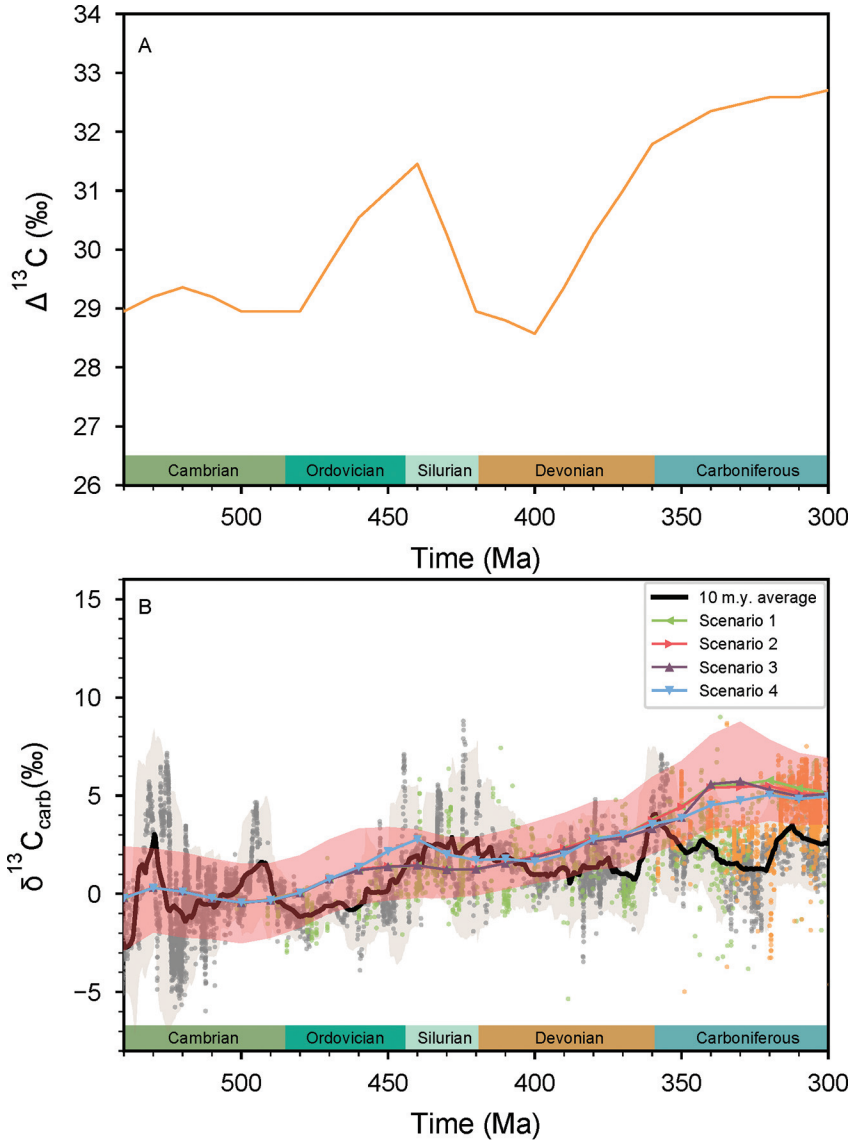

Fig. 9. $\Delta^{13}C$ from geological records and the carbonate $\delta^{13}C$ values required to reproduce the four oxygen scenarios using this $\Delta^{13}C$ formulation. (A) $\Delta^{13}C$ derived from Hayes and others (1999) through the Paleozoic. (B) The carbonate $\delta^{13}C$ required to reproduce the four oxygen scenarios using the $\Delta^{13}C$ derived from Hayes and others (1999). The symbols are described in figure 6. Different scenarios are described in figure 4.

atmospheric oxygen are equally or even more reasonable. Specifically, low atmospheric oxygen levels are also likely when there is a low initial sulfate proportion in the crust (for example, 20%). Therefore, although it is difficult with the current carbon isotope record to accurately predict atmospheric oxygen levels, GEOCARBSULF modeling can be consistent with the idea that the Paleozoic was a time of low atmospheric oxygen, and that land plants drove a step change in surface oxygen levels.

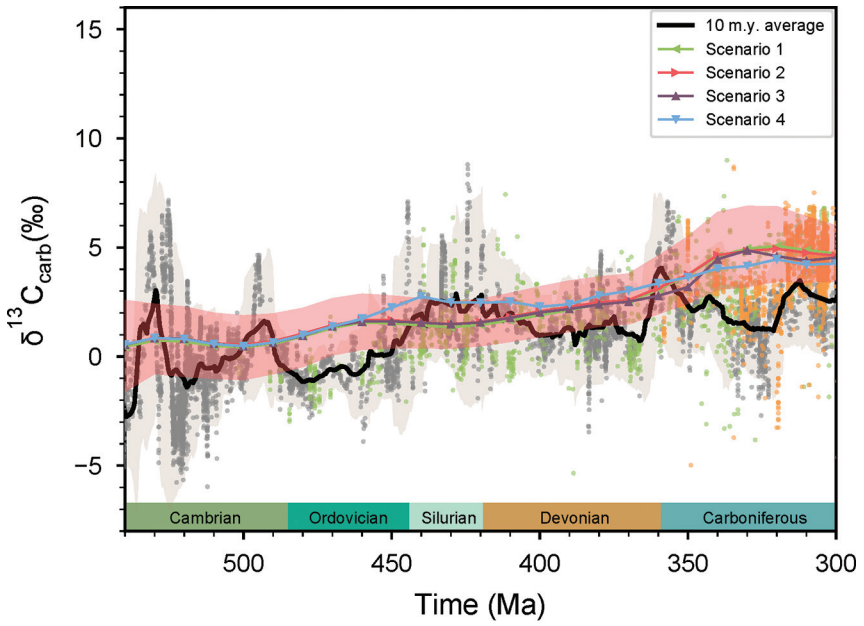

Fig. 10. The carbonate $\delta^{13}C$ required to reproduce the four oxygen scenarios through the Paleozoic, assuming 20% initial sulfate in the crust, and how they correlate with the geologic record. The symbols are described in figure 6. Different scenarios are described in figure 4.

A renewed effort to track carbon isotope gradients (following on from Holmden and others, 1998) and careful screening of samples for diagenetic alteration are essential to build a better global $\delta^{13}C$ trend in the Paleozoic, which may then contribute to a tighter constraint on the O_2 evolution predicted by GEOCARBSULF.

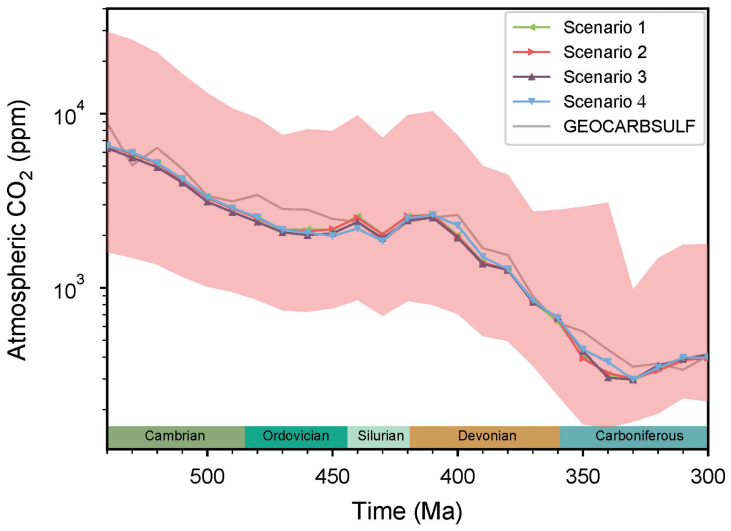

Fig. 11. Atmospheric CO_2 predicted in the sensitivity tests of carbonate $\delta^{13}C$ for different scenarios assuming 20% initial sulfate in the crust, compared with the CO_2 predicted from the original GEOCARBSULF (Royer and others, 2014). Different scenarios are described in figure 4.

CONCLUSIONS

We show that by altering the carbonate $\delta^{13}C$ within permissible bounds, as well as revising the sulfate/sulfide ratio of the upper crust at the Precambrian-Cambrian boundary, GEOCARBSULF can be consistent with the idea that the early Paleozoic was a time of low atmospheric oxygen, and that land plants drove a step change in surface oxygen levels. However, given the complexity of the carbonate $\delta^{13}C$ record, we also argue that uncertainties still exist in the prediction of atmospheric O_2 levels using GEOCARBSULF and more accurate predictions will come from an improved C isotope record.

ACKNOWLEDGMENTS

We thank Ellen Thomas for the carbonate $\delta^{13}C$ data. We thank Pincelli M. Hull for helpful discussions. Noah J. Planavsky acknowledges funding from the Alternative Earths NASA Astrobiology Institute and the Packard Foundation. Alexander J. Krause is funded by a UK NERC studentship. Edward W. Bolton acknowledges support from the Virtual Planetary Laboratory. Benjamin J. W. Mills is funded by a University of Leeds Academic Fellowship. We thank Lee Kump and two anonymous reviewers for their inputs in improving the manuscript. Noah J Planavsky is extermely grateful to Bob Berner for sharing insights from his decades of exploration of the BLAG family of models.

APPENDIX
MODEL BASED PALEOZOIC ATMOSPHERIC OXYGEN ESTIMATES: A REVISIT TO GEOCARBSULF

FULL MODEL DESCRIPTION

The original R code for GEOCARBSULF (Royer and others, 2014) can be found at https://figshare.com/articles/code_to_run_GEOCARBSULF_model/902207. The codes of sensitivity tests with GEOCARBSULF are hosted in https://github.com/wadesnoopy/MODEL-BASED-PALEOZOIC-ATMOSPHERIC-OXYGEN-ESTIMATES. The full model parameters and equations are as follows. More information (for example, 2SD for all parameters and the value of the time-dependent parameters) can be found in tables A7 and A8 in the Supplementary data file: http://earth.geology.yale.edu/%7eajs/SupplementaryData/2018/Zhang.

TABLE A1

Present day parameters

Parameter	Algebraic Representation	Value	Source
Atmosphere and ocean O_2	O_0	3.8×10^{19} mol	Royer and others (2014)
Sulfur flux from weathering of old pyrite	F_{wpa}_0	2.5×10^{17} mol	Royer and others (2014)
Sulfur flux from weathering of old gypsum	F_{wsa}_0	5×10^{17} mol/m.y	Royer and others (2014)
Carbon flux from weathering of old organic matter	F_{wga}_0	5×10^{17} mol/m.y	Royer and others (2014)
Carbon flux from weathering of old carbonate	F_{wca}_0	2×10^{18} mol/m.y	Royer and others (2014)
Carbon degassing flux from volcanism, metamorphism, and diagenesis of organic carbon	F_{mg}_0	1.25×10^{18} mol/m.y	Berner (2004)
Carbon degassing flux from volcanism, metamorphism, and diagenesis of carbonate	F_{mc}_0	6.67×10^{18} mol/m.y	Berner (2004)
Sulfur degassing flux from volcanism, metamorphism, and diagenesis of pyrite	F_{mp}_0	2.5×10^{17} mol/m.y	Royer and others (2014)
Sulfur degassing flux from volcanism, metamorphism, and diagenesis of gypsum	F_{ms}_0	5×10^{17} mol/m.y	Royer and others (2014)
Silicate weathering	F_{wsi}_0	6.67×10^{18} mol/m.y	Berner (1991)
Fraction of total Ca and Mg silicate weathering derived from volcanic rocks	X_{volc}_0	0.35	Berner (2006a, 2008)
Carbon isotopic fractionation between shallow-marine carbonate and organic carbon	$\Delta^{13}C\_0$	27	Berner (2006b)
Sulfur isotopic fractionation between shallow-marine gypsum sulfur and pyrite sulfur	$\Delta^{34}S\_0$	35	Berner (2006b)
Ca and Mg flux between basalt and seawater	F_{ob}_0	4×10^{18} mol/m.y	Berner (2008)

TABLE A2

Starting reservoir sizes and isotope ratios (570 Ma)

Parameter	Algebraic Representation	Value	Source
Young organic carbon	G_y_570	250×10^{18} mol	Berner (2006b)
Young carbonate	C_y_570	1000×10^{18} mol	Berner (2006b)
Young pyrite sulfur	P_y_570	20×10^{18} mol	Berner (2006b)
Young gypsum sulfur	S_y_570	150×10^{18} mol	Berner (2006b)
$\delta^{13}C$ of young organic carbon	dlgy_570	-23.5	Berner (2006b)
$\delta^{13}C$ of old organic carbon	dlga_570	-23.5	Berner (2006b)
$\delta^{13}C$ of young carbonate carbon	dlcy_570	3	Berner (2006b)
$\delta^{34}S$ of young pyrite sulfur	dlpy_570	-10	Berner (2006b)
$\delta^{34}S$ of old pyrite sulfur	dlpa_570	-10	Berner (2006b)
$\delta^{34}S$ of young gypsum sulfur	dlsy_570	35	Berner (2006b)
$^{87}Sr/^{86}Sr$ of young carbonates undergoing weathering	R_{cy}_570	0.7095	Royer and others (2014)
$^{87}Sr/^{86}Sr$ of old carbonates undergoing weathering	R_{ca}_570	0.709	Royer and others (2014)
$^{87}Sr/^{86}Sr$ of non-volcanic silicates	R_g_570	0.722	Berner (2008)

TABLE A3

Constant Parameters

Parameter	Algebraic Representation	Value	Source
Normalized activation energy for silicates	ACT_{si}	0.09 K^{-1}	Berner (2004)
Normalized activation energy for carbonates	ACT_{ca}	0.087 K^{-1}	Berner (2004)
Rate of chemical weathering in volcanic silicate rocks relative to non-volcanic silicate rocks	VNV	5	Berner (2006a, 2008)
Coefficient relating physical erosion to the mean $^{87}Sr/^{86}Sr$ of non-volcanic silicate rocks	NV	0.0075	Berner (2008)
Exponent relating physical erosion to the mean $^{87}Sr/^{86}Sr$ of non-volcanic silicate rocks	exp_NV	0.67	Berner (2008)
Rate of chemical weathering in a minimally-vegetated world relative to present-day	LIFE	0.25	Berner (2004)
Rate of chemical weathering by gymnosperms relative to angiosperms	GYM	0.875	Berner and Kothavala (2001)
Exponent reflecting the fraction of vegetation whose growth is stimulated by elevated CO_2	FERT	0.4	Berner and Kothavala (2001)
Exponent used to describe the effect of climate on silicate or carbonate weathering in the absence of vascular plants at time (t) relative to the present-day	exp_fnBb	0.5	Berner (1994, 2004)
Climate sensitivity	deltaT2X	3	Park and Royer (2011); Rohling and others (2012)
Factor by which deltaT2X changes during times with large continental ice sheets	GLAC	2	Park and Royer (2011); Rohling and others (2012)
Coefficient used to calculate CAPd13C	J	4‰	Berner (2006b)
Exponent used to calculate CAPd34S	n	1	Berner (2006b)
Effect on temperature from the linear increase in solar luminosity over time	Ws	7.4 k/570 m.y.	Berner (2004)
Exponent that scales the dilution of dissolved HCO_3^- with runoff	exp_fD	0.65	Berner (1994, 2004)
Mass of carbon in ocean	COC	2×10^{18} mol	Royer and others (2014)
Mass of old organic carbon	G_a	1000×10^{18} mol	Berner (2006b)
Mass of old carbonate carbon	C_a	4000×10^{18} mol	Berner (2006b)
Mass of old pyrite sulfur	P_a	280×10^{18} mol	Berner (2006b)

TABLE A3
(continued)

Parameter	Algebraic Representation	Value	Source
Mass of old gypsum sulfur	S_a	150×10^{18} mol	Berner (2006b)
Mass of carbon in oceans + "interacting rocks"	CT	4252×10^{18} mol	Royer and others (2014)
$\delta^{13}C$ of CT	dlct	-3.5‰	Royer and others (2014)
Mass of sulfur in oceans + "interacting rocks"	ST	600×10^{18} mol	Royer and others (2014)
$\delta^{34}S$ of CT	dlst	4‰	Royer and others (2014)
Rate constant expressing mass dependence for young pyrite sulfur	k_{wpy}	0.01/m.y.	Berner (2006b)
Rate constant expressing mass dependence for young gypsum sulfur	k_{wsy}	0.01/m.y.	Berner (2006b)
Rate constant expressing mass dependence for young organic carbon weathering	k_{wgy}	0.018/m.y.	Berner (2006b)
Rate constant expressing mass dependence for young carbonate weathering	k_{wcy}	0.018/m.y.	Berner (2006b)
$^{87}Sr/^{86}Sr$ of volcanic rocks	R_v	0.704	Berner (2008)

TABLE A4

Time dependent parameters

Parameter	Algebraic Representation	Source	Notes
Strontium isotopic composition of shallow-marine carbonate [($^{87}Sr/^{86}Sr$-0.7)*10^4]	Sr	Berner (1994; 2004)	See table A8
Carbon isotopic composition of shallow marine carbonate	$\delta^{13}C$	Berner (2004; 2006b; 2009)	See table A8
Sulfur isotopic composition of shallow-marine carbonate	$\delta^{34}S$	Wu and others (2010)	See table A8
Effect of relief on chemical weathering at time (t) relative to the present-day	f_R	Berner (2004)	See table A8
Land area covered by carbonates at time (t) relative to the present-day	f_L	Berner (2004); Bluth and Kump (1991)	See table A8
Land area at time (t) relative to the present-day	f_A	Berner (2004); Otto-Bliesner (1995); Goddéris and others (2012)	See table A8
Global river runoff at time (t) relative to the present-day in the absence of changes in solar luminosity and CO_2	f_D	Berner (2004); Otto-Bliesner (1995); Goddéris and others (2012)	See table A8
Fraction of land area undergoing chemical weathering	$f_{Aw}\_f_A$	Goddéris and others (2012)	See table A8
Coefficient of continental runoff versus temperature change	RT	Goddéris and others (2012)	See table A8
Change in land mean surface temperature that is undergoing chemical weathering at time (t) relative to the present-day in the absence of changes in solar luminosity and CO_2	GEOG	Berner (2004); Otto-Bliesner (1995); Goddéris and others (2012)	See table A8
Seafloor creation rate at time (t) relative to the present-day	f_{SR}	Berner (2004)	See table A8
Effect of carbonate content of subducting oceanic crust on CO_2 degassing rate at time (t) relative to the present-day	f_C	Berner (2004)	See table A8

TABLE A5

Flux and parameter equations

Parameter	Equation	
Ratio of O_2 relative to present day	$RO_2 = \frac{O_2(t)}{O0}$	(1)
Conversion of absolute mass of O_2 (in 10^{18} mol) to atmospheric %	$O_2\_atm = \left(\frac{O_2(t)}{O_2(t)+143}\right)\cdot 100$	(2)
Direct effect of atmospheric CO_2 on weathering rate of carbonate and silicate (applied to period before rise of large land plants at 380 Ma)	$f_{Bnb} = RCO_2^{\exp\_fnBb}$	(3)
Effect of CO_2 on plant-assisted weathering of silicates and carbonates	$f_{Bb} = \left(\frac{2\cdot RCO_2}{1+RCO_2}\right)^{FERT}$	(4)
Effect of atmospheric CO_2 on weathering rate of carbonate and silicate (in the absence of its effect on temperature)	$f_{CO_2} = f_{Bnb}\ (570\text{–}380\ Ma)$ $f_{CO_2} = f_{Bb}\ (350\text{–}0\ Ma)$ Linear interpolation between 380–350 Ma	(5)
Effect of plants on weathering rate of silicates and carbonates	$f_E = LIFE\ (570\text{–}380\ Ma)$ $f_E = GYM\ (350\text{–}130\ Ma)$ $f_E = 1\ \ (80\text{–}0\ Ma)$ Linear interpolation between 380–350 Ma and 130–80 Ma	(6)
Global average temperature relative to present	$temp = \left(GLAC \times \frac{deltaT2X}{ln2} \times ln\, RCO_2\right) - \left(Ws \cdot \frac{t}{570}\right) + GEOG$ (for glacial periods between 260 and 330 Ma and between 40 and 0 Ma) $temp = \left(\frac{deltaT2X}{ln2} \times ln\, RCO_2\right) - \left(Ws \cdot \frac{t}{570}\right) + GEOG$ (for other time periods)	(7)

TABLE A5

(continued)

Parameter	Equation	
Effect of changes in temperature on silicate weathering	$f_{wsi\_T} = e^{(ACT_{si} \cdot temp)} \cdot [1 + (RT \cdot temp)]^{exp\_fD}$	(8)
Effect of changes in temperature on carbonate weathering	$f_{wca\_T} = 1 + ACT_{ca} \cdot temp$	(9)
Combined effect of changes to temperature and CO_2 on silicate weathering	$f_{Bb\_si} = f_{wsi\_T} \cdot f_{CO_2}$	(10)
Combined effect of changes to temperature and CO_2 on carbonate weathering	$f_{Bb\_ca} = f_{wca\_T} \cdot f_{CO_2}$	(11)
Weathering of young organic carbon	$F_{wgy} = f_A \cdot f_R \cdot k_{wgy} \cdot G_y(t)$	(12)
Weathering of old organic carbon	$F_{wga} = f_R \cdot F_{wga\_}0$	(13)
Weathering of young carbonate	$F_{wcy} = f_A \cdot f_D \cdot f_L \cdot f_E \cdot f_{Bb\_ca} \cdot k_{wcy} \cdot C_y(t)$	(14)
Weathering of old carbonate	$F_{wca} = f_A \cdot f_D \cdot f_L \cdot f_E \cdot f_{Bb\_ca} \cdot F_{wca\_}0$	(15)
Weathering of young pyrite	$F_{wpy} = f_A \cdot f_R \cdot k_{wpy} \cdot P_y(t)$	(16)
Weathering of ancient pyrite	$F_{wpa} = f_R \cdot F_{wpa\_}0$	(17)
Weathering of young gypsum	$F_{wsy} = f_A \cdot f_D \cdot k_{wsy} \cdot S_y(t)$	(18)
Weathering of ancient gypsum	$F_{wsa} = f_A \cdot f_D \cdot F_{wsa\_}0$	(19)
Metamorphism / degassing of organic carbon	$F_{mg} = f_{SR} \cdot F_{mg\_}0$	(20)
Metamorphism / degassing of carbonate	$F_{mc} = f_{SR} \cdot f_C \cdot F_{mc\_}0$	(21)
Metamorphism / degassing of pyrite sulfur	$F_{mp} = f_{SR} \cdot F_{mp\_}0$	(22)

TABLE A5
(continued)

Parameter	Equation	
Metamorphism/degassing of gypsum sulfur	$F_{ms} = f_{SR} \cdot F_{ms\_}0$	(23)
Organic carbon transfer from young to old reservoir	$F_{yog} = F_{wga} + F_{mg}$	(24)
Carbonate transfer from young to old reservoir	$F_{yoc} = F_{wca} + F_{mc}$	(25)
Pyrite sulfur transfer from young to old reservoir	$F_{yop} = F_{wpa} + F_{mp}$	(26)
Gypsum sulfur transfer from young to old reservoir	$F_{yos} = F_{wsa} + F_{ms}$	(27)
Fractionation of $\delta^{13}C$ between carbonate and organic matter	$\Delta^{13}\mathrm{C} = \Delta^{13}\mathrm{C\_0} + [J \cdot (RO_2 - 1)]$	(28)
Fractionation of $\delta^{34}S$ between sulfate sulfur and pyrite sulfur	$\Delta^{34}\mathrm{S} = \Delta^{34}\mathrm{S\_0} \times {RO_2}^n$	(29)
Burial of organic carbon	$F_{bg} = \frac{1}{\Delta^{13}\mathrm{C}} \times \left[(\delta^{13}\mathrm{C} - \mathrm{dlcy}) \cdot \mathrm{F_{wcy}} + (\delta^{13}\mathrm{C} - \mathrm{dlca}) * \mathrm{F_{wca}} + (\delta^{13}\mathrm{C} - \mathrm{dlgy}) * \mathrm{F_{wgy}} + (\delta^{13}\mathrm{C} - \mathrm{dlga}) * \mathrm{F_{wga}} + (\delta^{13}\mathrm{C} - \mathrm{dlca}) * \mathrm{F_{mc}} + (\delta^{13}\mathrm{C} - \mathrm{dlga}) * \mathrm{F_{mg}}\right]$	(30)
Burial of carbonate	$F_{bc} = \mathrm{F_{wgy}} + \mathrm{F_{wga}} + \mathrm{F_{wcy}} + \mathrm{F_{wca}} + \mathrm{F_{mg}} + \mathrm{F_{mc}} - F_{bg}$	(31)
Burial of pyrite	$F_{bp} = \frac{1}{\Delta^{34}\mathrm{S}} \times \left[(\delta^{34}\mathrm{S} - \mathrm{dlsy}) \cdot \mathrm{F_{wsy}} + (\delta^{34}\mathrm{S} - \mathrm{dlsa}) * \mathrm{F_{wsa}} + (\delta^{34}\mathrm{S} - \mathrm{dlpy}) * \mathrm{F_{wpy}} + (\delta^{34}\mathrm{S} - \mathrm{dlpa}) * \mathrm{F_{wpa}} + (\delta^{34}\mathrm{S} - \mathrm{dlsa}) * \mathrm{F_{ms}} + (\delta^{34}\mathrm{S} - \mathrm{dlpa}) * \mathrm{F_{mp}}\right]$	(32)
Burial of gypsum	$F_{bs} = \mathrm{F_{wpy}} + \mathrm{F_{wpa}} + \mathrm{F_{wsy}} + \mathrm{F_{wsa}} + \mathrm{F_{mp}} + \mathrm{F_{ms}} - F_{bp}$	(33)

TABLE A5
(continued)

Parameter	Equation	
Silicate weathering determined from mass balance	$F_{wsi} = \mathrm{F_{bc}} - \mathrm{F_{wcy}} - \mathrm{F_{wca}}$	(34)
Convert strontium isotopes to $^{87}Sr/^{86}Sr$	$R_{OC} = \frac{Sr}{10000} + 0.7$	(35)
Strontium fractionation of non-volcanic silicates:	$R_g = R_g\_570 - NV \cdot \left(1 - f_R^{\frac{1}{exp\_NV}}\right)$	(36)
Fraction of total Ca and Mg silicate weathering derived from volcanic rocks	$X_{volc} = \{[f_{SR} \cdot f_{ob}\_0 \cdot (R_v - R_{oc})] + (F_{wcy} \cdot R_{cy}) + (F_{wca} \cdot R_{ca}) - (R_{oc} \cdot F_{bc}) + (R_g \cdot F_{wsi})\}/F_{wsi} \cdot (R_g - R_v)$	(37)
Volcanic weathering effect	$f_{volc} = \frac{(VNV \cdot X_{volc}) + (1 - X_{volc})}{(VNV \cdot X_{volc}\_0) + (1 - X_{volc}\_0)}$	(38)
Silicate weathering determined from geological processes	$F_{wsi} = f_{volc} \cdot f_{Bb\_si} \cdot f_{AW}\_f_A \cdot (f_A \cdot f_D)^{exp\_fD} \cdot f_R \cdot f_E \cdot F_{wsi}\_0$	(39)

TABLE A6

Reservoir equations

Parameter	Reservoir Equation	
Atmospheric oxygen	$\frac{dO_2}{dt} = \left[F_{bg} + \left(\frac{15}{8} \cdot F_{bp}\right)\right] - \left(F_{wgy} + F_{wga} + F_{mg}\right) - \left[\frac{15}{8} \cdot \left(F_{wpy} + F_{wpa} + F_{mp}\right)\right]$	(40)
Young organic carbon	$\frac{dG_y}{dt} = F_{bg} - F_{wgy} - F_{yog}$	(41)
Young carbonate carbon	$\frac{dC_y}{dt} = F_{bc} - F_{wcy} - F_{yoc}$	(42)
Young pyrite sulfur	$\frac{dP_y}{dt} = F_{bp} - F_{wpy} - F_{yop}$	(43)
Young gypsum sulfur	$\frac{dS_y}{dt} = F_{bs} - F_{wsy} - F_{yos}$	(44)
Young organic carbon isotope mass balance	$\frac{d(dlgy \cdot G_y)}{dt} = \left[(\delta^{13}C - \Delta^{13}C) \cdot F_{bg}\right] - \left(dlgy \cdot F_{wgy}\right) - \left(dlgy \cdot F_{yog}\right)$	(45)
Old organic carbon isotope mass balance	$\frac{d(dlga \cdot G_a)}{dt} = \left(dlgy \cdot F_{yog}\right) - \left(dlga \cdot F_{wga}\right) - \left(dlga \cdot F_{mg}\right)$	(46)
Young carbonate carbon isotope mass balance	$\frac{d(dlcy \cdot C_y)}{dt} = (\delta^{13}C \cdot F_{bc}) - \left(dlcy \cdot F_{wcy}\right) - \left(dlcy \cdot F_{yoc}\right)$	(47)
Old carbonate carbon isotope mass balance	$\frac{d(dlca \cdot C_a)}{dt} = \left(dlcy \cdot F_{yoc}\right) - (dlca \cdot F_{wca}) - (dlca \cdot F_{mc})$	(48)
Young pyrite sulfur isotope mass balance	$\frac{d(dlpy \cdot P_y)}{dt} = \left[(\delta^{34}S - \Delta^{34}S) \cdot F_{bp}\right] - \left(dlpy \cdot F_{wpy}\right) - \left(dlpy \cdot F_{yop}\right)$	(49)
Old pyrite sulfur isotope mass balance	$\frac{d(dlpa \cdot P_a)}{dt} = \left(dlpy \cdot F_{yop}\right) - \left(dlpa \cdot F_{wpa}\right) - \left(dlpa \cdot F_{mp}\right)$	(50)
Young gypsum sulfur isotope mass balance	$\frac{d(dlsy \cdot S_y)}{dt} = (\delta^{34}S \cdot F_{bs}) - \left(dlsy \cdot F_{wsy}\right) - \left(dlsy \cdot F_{yos}\right)$	(51)
Old gypsum sulfur isotope mass balance	$\frac{d(dlsa \cdot S_a)}{dt} = \left(dlsy \cdot F_{yos}\right) - (dlsa \cdot F_{wsa}) - (dlsa \cdot F_{ms})$	(52)
$^{87}Sr/^{86}Sr$ of young carbonate undergoing weathering	$\frac{d(R_{cy} \cdot C_y)}{dt} = (R_{oc} \cdot F_{bc}) - \left(R_{cy} \cdot F_{wcy}\right) - \left(R_{cy} \cdot F_{yoc}\right)$	(53)
$^{87}Sr/^{86}Sr$ of old carbonate undergoing weathering	$\frac{d(R_{ca} \cdot C_a)}{dt} = \left(R_{cy} \cdot F_{yoc}\right) - (R_{ca} \cdot F_{wca}) - (R_{ca} \cdot F_{mc})$	(54)

The reservoir equations are solved using a finite difference method from 570 to 0 Ma, with a time step of 10 million years. Note that there is no differential equation for the old reservoir (Ga, Ca, Pa and Sa) because their mass is fixed through time in GEOCARBSULF. Note that there is no ordinary differential equation for atmospheric CO_2. This is because CO_2 in the GEOCARBSULF is not solved explicitly using the finite difference method. Since carbonate burial is equal to carbonate weathering plus silicate weathering on a time scale of 10 million years, its value is obtained by solving a non-linear equation which contains RCO_2 at each time step, as follows:

$$F_{bc} - F_{wcy} - F_{wca} = f_{volc} \cdot f_{Bb\_si} \cdot f_{AW\_fA} \cdot (f_A \cdot f_D)^{exp\_fD} \cdot f_R \cdot f_E \cdot \mathrm{Fwsi\_0} \quad (55)$$

SENSITIVITY TESTS OF CARBONATE $\Delta^{13}C$ ON O_2 LEVELS THROUGH THE WHOLE PHANEROZOIC

We also calculated the required $\delta^{13}C$ over the whole Phanerozoic, again taking a range of estimates for oxygen concentrations from 570 to 0 Ma (fig. A1). From 570 to 300 Ma, the O_2 evolution follows the four scenarios in figure 4. From 300 to 0 Ma, the O_2 evolution follows three scenarios, including the O_2 output from the original GEOCARBSULF (GEOCARBSULF), O_2 output from the original COPSE (COPSE) and O_2 remaining at 21% (fix21). Scenario 1-GEOCABRSULF means the original Scenario 1 followed by GEOCARBSULF, Scenario 1-COPSE means the original Scenario 1 followed by COPSE and Scenario 1-fix21 means the original Scenario 1 followed by fix21. The same terminology applies to Scenario 2. Scenario 3 means the original Scenario 3 followed by COPSE and Scenario 4 means the original Scenario 4 followed by COPSE. Using the same method, similarly, the required $\delta^{13}C$ is close to the range observed in data compilations (fig. A2).

IMPLEMENTATION OF THE INTEGRATED LAND-SURFACE OXIDATIVE WEATHERING MODEL INTO GEOCARBSULF

At low atmospheric O_2 levels (less than 18% PAL), the weathering of organic carbon is thought to be incomplete and the weathering extent is argued to scale with O_2 levels (Bolton and others, 2006). This incomplete oxidative weathering model has been shown to accurately reconstruct modern black shale profiles (Bolton and others, 2006). Assuming this is right, the fixed weathering rate of organic carbon (per Myr) formulated in GEOCARBSULF may exaggerate the organic carbon weathering rate when O_2 level is low (as in the Cambrian).

To explore the influence of O_2 levels on organic carbon weathering rates, which in turn affects the model predictions of O_2 levels, we integrated the land-surface oxidative weathering model (Bolton, personal communication) into GEOCARBSULF. We assume the global erosion rate is 5cm/kyr (Lasaga and Ohmoto, 2002) and the organic carbon content at depth is 0.6 wt. %, from which the oxidation percentage of organic carbon at the surface can be calculated (fig. A3). Afterwards, we add the percentage value ($S_{weather}$) to scale the weathering rate of organic matter as follows:

F_{wgy}: carbon flux from weathering of young organic carbon

$$F_{wgy} = S_{weather} \cdot f_A \cdot f_R \cdot \mathrm{k_{wgy}} \cdot G_y(t) \quad (56)$$

F_{wga}: carbon flux from weathering of old organic carbon

$$F_{wga} = S_{weather} \cdot f_R \cdot F_{wga\_0} \quad (57)$$

Following this modification, we calculated the $\delta^{13}C$ values required to produce the example O_2 curves. GEOCARBSULF shows that incomplete organic carbon weathering had a limited effect on atmospheric oxygen levels (fig. A4).

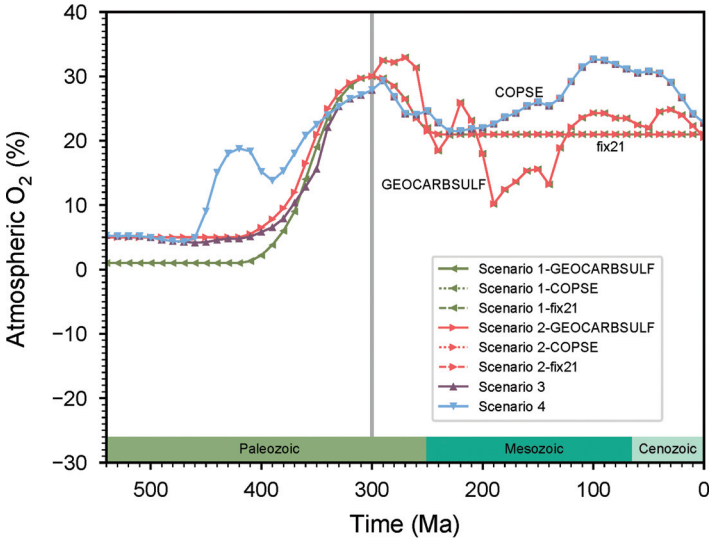

Fig. A1. Atmospheric O_2 evolution scenarios through the Phanerozoic. Scenario 1, 2, 3, 4 are described in figure 4. The suffix (that is, GEOCARBSULF, COPSE, fix21) represents the O_2 evolution from 300 Ma to present reconstructed by different model approaches and assumptions. "GEOCARBSULF" means the standard O_2 curve from Royer and others (2014), "COPSE" means the baseline O_2 curve from Bergman and others (2004), and "fix21" means the O_2 level dropped from 300 to 240 Ma smoothly and remained constant at 21% afterwards until 0 Ma.

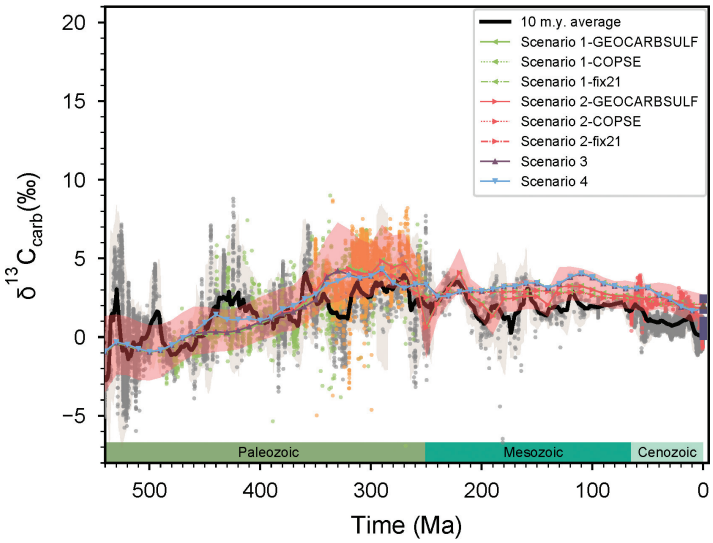

Fig. A2. Carbonate $\delta^{13}C$ required to reproduce the four oxygen scenarios through the Paleozoic, and how they correlate with the geologic record. The red dots are the bulk carbonate $\delta^{13}C$ values from Katz and others (2005). The purple squares from high to low represent the pre-industrial $\delta^{13}C$ values of DIC in the low-latitude surface ocean of the Atlantic, the low-latitude surface ocean of the Indian Ocean, the low-latitude surface ocean of the Pacific, the intermediate ocean of the Atlantic, the intermediate ocean of the Indian Ocean, the intermediate ocean of Pacific, the deep ocean of the Atlantic, the deep ocean of the Indian Ocean, the deep ocean of the Pacific, and the high-latitude surface ocean respectively calculated using LOSCAR (Zeebe, 2012). The brown triangles represents the pre-industrial $\delta^{13}C$ values of bicarbonate ions in the ocean (Zeebe and Wolf-Gladrow, 2001). The other symbols are described in figure 6. Different scenarios are described in figure 4.

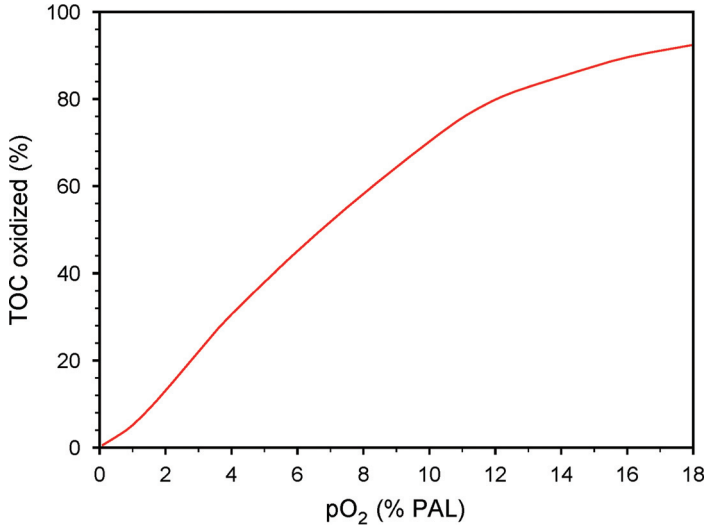

Fig. A3. Total organic carbon (TOC) in the top layer of the rock oxidized as a function of the atmospheric O_2 level. Note that the erosion rate is 5 cm/kyr and the initial organic carbon content is 0.6 wt. % for this curve.

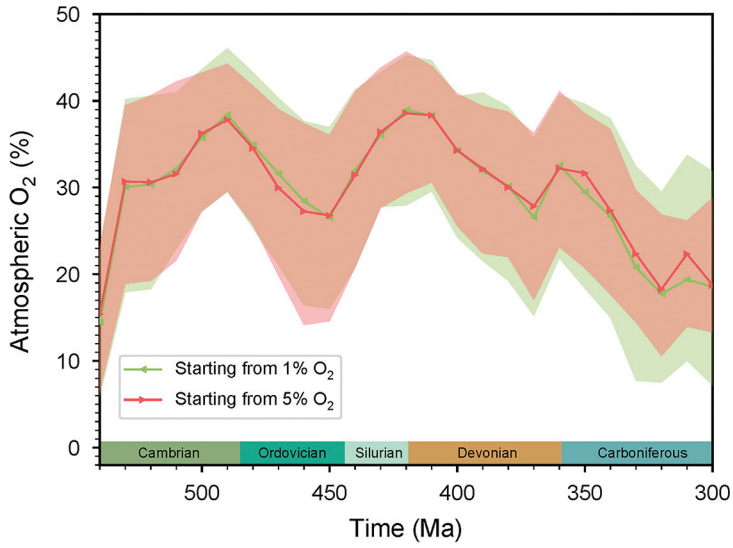

Fig. A4. Outputs from the GEOCARBSULF model assuming different initial O_2 levels by integrating the land-surface oxidative weathering model.

REFERENCES

Arvidson, R. S., Mackenzie, F. T., and Guidry, M. W., 2013, Geologic history of seawater: A *MAG*ic approach to carbon chemistry and ocean ventilation: Chemical Geology, v. 362, p. 287–304, https://doi.org/10.1016/j.chemgeo.2013.10.012

Beerling, D. J., Lake, J. A., Berner, R. A., Hickey, L. J., Taylor, D. W., and Royer, D. L., 2002, Carbon isotope evidence implying high O_2/CO_2 ratios in the Permo-Carboniferous atmosphere: Geochimica et Cosmochimica Acta, v. 66, n. 21, p. 3757–3767, https://doi.org/10.1016/S0016-7037(02)00901-8

Belcher, C. M., and McElwain, J. C., 2008, Limits for combustion in low O_2 redefine paleoatmospheric predictions for the Mesozoic: Science, v. 321, n. 5893, p. 1197–1200, https://doi.org/10.1126/science.1160978

Bergman, N. M., Lenton, T. M., and Watson, A. J., 2004, COPSE: A new model of biogeochemical cycling over Phanerozoic time: American Journal of Science, v. 304, n. 5, p. 397–437, https://doi.org/10.2475/ajs.304.5.397

Berner, R. A., 1987, Models for carbon and sulfur cycles and atmospheric oxygen: Application to Paleozoic geologic history: American Journal of Science, v. 287, n. 3, p. 177–196, https://doi.org/10.2475/ajs.287.3.177

——— 1991, A model for atmospheric CO_2 over Phanerozoic time: American Journal of Science, v. 291, n. 4, p. 339–376, https://doi.org/10.2475/ajs.291.4.339

——— 1994, GEOCARB II: A revised model of atmospheric CO_2 over Phanerozoic time: American Journal of Science, v. 294, n. 1, p. 56–91, https://doi.org/10.2475/ajs.294.1.56

——— 2001, Modeling atmospheric O_2 over Phanerozoic time: Geochimica et Cosmochimica Acta, v. 65, n. 5, p. 685–694, https://doi.org/10.1016/S0016-7037(00)00572-X

——— 2004, The Phanerozoic Carbon Cycle: CO_2 and O_2: New York, Oxford University Press, 158 p.

——— 2006a, Inclusion of the Weathering of Volcanic Rocks in the GEOCARBSULF Model: American Journal of Science, v. 306, n. 5, p. 295–302, https://doi.org/10.2475/05.2006.01

——— 2006b, GEOCARBSULF: A combined model for Phanerozoic atmospheric O_2 and CO_2: Geochimica et Cosmochimica Acta, v. 70, n. 23, p. 5653–5664, https://doi.org/10.1016/j.gca.2005.11.032

——— 2008, Addendum to "Inclusion of the Weathering of Volcanic Rocks in the GEOCARBSULF Model" (R. A. Berner, 2006, V. 306, p. 295–302): American Journal of Science, v. 308, n. 1, p. 100–103, https://doi.org/10.2475/01.2008.04

——— 2009, Phanerozoic atmospheric oxygen: New results using the GEOCARBSULF model: American Journal of Science, v. 309, n. 7, p. 603–606, https://doi.org/10.2475/07.2009.03

Berner, R. A., and Canfield, D. E., 1989, A new model for atmospheric oxygen over Phanerozoic time: American Journal of Science, v. 289, n. 4, p. 333–361, https://doi.org/10.2475/ajs.289.4.333

Berner, R. A., and Kothavala, Z., 2001, Geocarb III: A Revised Model of Atmospheric CO_2 over Phanerozoic Time: American Journal of Science, v. 301, n. 2, p. 182–204, https://doi.org/10.2475/ajs.301.2.182

Berner, R. A., Petsch, S. T., Lake, J. A., Beerling, D. J., Popp, B. N., Lane, R. S., Laws, E. A., Westley, M. B., Cassar, N., Woodward, F. I., and Quick, W. P., 2000, Isotope Fractionation and Atmospheric Oxygen: Implications for Phanerozoic O_2 Evolution: Science, v. 287, n. 5458, p. 1630–1633, https://doi.org/10.1126/science.287.5458.1630

Bluth, G. J. S., and Kump, L. R., 1991, Phanerozoic paleogeology: American Journal of Science, v. 291, n. 3, p. 284–308, https://doi.org/10.2475/ajs.291.3.284

Bolton, E. W., Berner, R. A., and Petsch, S. T., 2006, The Weathering of Sedimentary Organic Matter as a Control on Atmospheric O_2: II. Theoretical Modeling: American Journal of Science, v. 306, n. 8, p. 575–615, https://doi.org/10.2475/08.2006.01

Brand, U., Tazawa, J., Sano, H., Azmy, K., and Lee, X., 2009, Is mid-late Paleozoic ocean-water chemistry coupled with epeiric seawater isotope records?: Geology, v. 37, n. 9, p. 823–826, https://doi.org/10.1130/G30038A.1

Canfield, D. E., 1998, A new model for Proterozoic ocean chemistry: Nature, v. 396, p. 450–453, https://doi.org/10.1038/24839

——— 2001, Biogeochemistry of Sulfur Isotopes: Reviews in Mineralogy and Geochemistry, v. 43, p. 607–636, https://doi.org/10.2138/gsrmg.43.1.607

Canfield, D. E., and Farquhar, J., 2009, Animal evolution, bioturbation, and the sulfate concentration of the oceans: Proceedings of the National Academy of Sciences of the United States of America, v. 106, n. 20, p. 8123–8127, https://doi.org/10.1073/pnas.0902037106

Dahl, T. W., Hammarlund, E. U., Anbar, A. D., Bond, D. P. G., Gill, B. C., Gordon, G. W., Knoll, A. H., Nielsen, A. T., Schovsbo, N. H., and Canfield, D. E., 2010, Devonian rise in atmospheric oxygen correlated to the radiations of terrestrial plants and large predatory fish: Proceedings of the National Academy of Sciences of the United States of America, v. 107, n. 42, p. 17911–17915, https://doi.org/10.1073/pnas.1011287107

Falkowski, P. G., Katz, M. E., Milligan, A. J., Fennel, K., Cramer, B. S., Aubry, M. P., Berner, R. A., Novacek, M. J., and Zapol, W. M., 2005, The Rise of Oxygen over the past 205 Million Years and the Evolution of Large Placental Mammals: Science, v. 309, n. 5744, p. 2202–2204, https://doi.org/10.1126/science.1116047

Garrels, R. M., and Lerman, A., 1981, Phanerozoic cycles of sedimentary carbon and sulfur: Proceedings of the National Academy of Sciences of the United States of America, v. 78, n. 8, p. 4652–4656, https://doi.org/10.1073/pnas.78.8.4652

——— 1984, Coupling of the sedimentary sulfur and carbon cycles: An improved model: American Journal of Science, v. 284, n. 9, p. 989–1007, https://doi.org/10.2475/ajs.284.9.989

Glasspool, I. J., Scott, A. C., Waltham, D., Pronina, N., and Shao, L., 2015, The impact of fire on the Late Paleozoic Earth system: Frontiers in Plant Science, v. 6, Article 756, https://doi.org/10.3389/fpls.2015.00756

Goddéris, Y., Donnadieu, Y., Lefebvre, V., Le Hir, G., and Nardin, E., 2012, Tectonic control of continental weathering, atmospheric CO_2, and climate over Phanerozoic times: Comptes Rendus Geoscience, v. 344, n. 11–12, p. 652–662, https://doi.org/10.1016/j.crte.2012.08.009

Grossman, E. L., Yancey, T. E., Jones, T. E., Bruckschen, P., Chuvashov, B., Mazzullo, S. J., and Mii, H., 2008, Glaciation, aridification, and carbon sequestration in the Permo-Carboniferous: The isotopic record from low latitudes: Palaeogeography, Palaeoclimatology, Palaeoecology, v. 268, n. 3–4, p. 222–233, https://doi.org/10.1016/j.palaeo.2008.03.053

Halevy, I., Peters, S. E., and Fischer, W. W., 2012, Sulfate Burial Constraints on the Phanerozoic Sulfur Cycle: Science, v. 337, n. 6092, p. 331–334, https://doi.org/10.1126/science.1220224

Hansen, K. W., and Wallmann, K., 2003, Cretaceous and Cenozoic evolution of seawater composition, atmospheric O_2 and CO_2: A model perspective: American Journal of Science, v. 303, n. 2, p. 94–148, https://doi.org/10.2475/ajs.303.2.94

Hayes, J. M., Strauss, H., and Kaufman, A. J., 1999, The abundance of ^{13}C in marine organic matter and isotopic fractionation in the global biogeochemical cycle of carbon during the past 800 Ma: Chemical Geology, v. 161, n. 1–3, p. 103–125, https://doi.org/10.1016/S0009-2541(99)00083-2

Holmden, C., Creaser, R. A., Muehlenbachs, K., Leslie, S. A., and Bergström, S. M., 1998, Isotopic evidence for geochemical decoupling between ancient epeiric seas and bordering oceans: Implications for secular curves: Geology, v. 26, n. 6, p. 567–570, https://doi.org/10.1130/0091-7613(1998)026<0567:IEFGDB>2.3.CO;2

Johnston, D. T., 2011, Multiple sulfur isotopes and the evolution of Earth's surface sulfur cycle: Earth-Science Reviews, v. 106, n. 1–2, p. 161–183, https://doi.org/10.1016/j.earscirev.2011.02.003

Katz, M. E., Wright, J. D., Miller, K. G., Cramer, B. S., Fennel, K., and Falkowski, P. G., 2005, Biological overprint of the geological carbon cycle: Marine Geology, v. 217, n. 3–4, p. 323–338, https://doi.org/10.1016/j.margeo.2004.08.005

Lasaga, A. C., and Ohmoto, H., 2002, The oxygen geochemical cycle: Dynamics and stability: Geochimica et Cosmochimica Acta, v. 66, n. 3, p. 361–381, https://doi.org/10.1016/S0016-7037(01)00685-8

Lenton, T. M., Dahl, T. W., Daines, S. J., Mills, B. J. W., Ozaki, K., Saltzman, M. R., and Porada, P., 2016, Earliest land plants created modern levels of atmospheric oxygen: Proceedings of the National Academy of Sciences of the United States of America, v. 113, n. 35, p. 9704–9709, https://doi.org/10.1073/pnas.1604787113

McKenzie, N. R., Horton, B. K., Loomis, S. E., Stockli, D. F., Planavsky, N. J., and Lee, C.-T. A., 2016, Continental arc volcanism as the principal driver of icehouse-greenhouse variability: Science, v. 352, n. 6284, p. 444–447, https://doi.org/10.1126/science.aad5787

Mii, H., Grossman, E. L., and Yancey, T. E., 1999, Carboniferous isotope stratigraphies of North America: Implications for Carboniferous paleoceanography and Mississippian glaciation: Geological Society of America Bulletin, v. 111, n. 7, p. 960–973, https://doi.org/10.1130/0016-7606(1999)111<0960:CISONA>2.3.CO;2

Mills, B., Daines, S. J., and Lenton, T. M., 2014, Changing tectonic controls on the long-term carbon cycle from Mesozoic to present: Geochemistry, Geophysics, Geosystems, v. 15, n. 12, p. 4866–4884, https://doi.org/10.1002/2014GC005530

Mills, B. J. W., Belcher, C. M., Lenton, T. M., and Newton, R. J., 2016, A modeling case for high atmospheric oxygen concentrations during the Mesozoic and Cenozoic: Geology, v. 44, n. 12, p. 1023–1026, https://doi.org/10.1130/G38231.1

Otto-Bliesner, B. L., 1995, Continental drift, runoff, and weathering feedbacks: Implications from climate model experiments: Journal of Geophysical Research: Atmospheres, v. 100, n. D6, p. 11537–11548, https://doi.org/10.1029/95JD00591

Panchuk, K. M., Holmden, C. E., and Leslie, S. A., 2006, Local Controls on Carbon Cycling in the Ordovician Midcontinent Region of North America, with Implications for Carbon Isotope Secular Curves: Journal of Sedimentary Research, v. 76, n. 2, p. 200–211, https://doi.org/10.2110/jsr.2006.017

Park, J., and Royer, D. L., 2011, Geologic constraints on the glacial amplification of Phanerozoic climate sensitivity: American Journal of Science, v. 311, n. 1, p. 1–26, https://doi.org/10.2475/01.2011.01

Rohling, E. J., Sluijs, A., Dijkstra, H. A., Köhler, P., van de Wal, R. S. W., von der Heydt, A. S., Beerling, D. J., Berger, A., Bijl, P. K., Crucifix, M., DeConto, R., Drijfhout, S. S., Fedorov, A., Foster, G. L., Ganopolski, A., Hansen, J., Hönisch, B., Hooghiemstra, H., Huber, M., Huybers, P., Knutti, R., Lea, D. W., Lourens, L. J., Lunt, D., Masson-Delmotte, V., Medina-Elizalde, M., Otto-Bliesner, B., Pagani, M., Pälike, H., Renssen, H., Royer, D. L., Siddall, M., Valdes, P., Zachos, J. C., and Zeebe, R. E., 2012, Making sense of palaeoclimate sensitivity: Nature, v. 491, p. 683–691, https://doi.org/10.1038/nature11574

Royer, D. L., Donnadieu, Y., Park, J., Kowalczyk, J., and Goddéris, Y., 2014, Error analysis of CO_2 and O_2 estimates from the long-term geochemical model GEOCARBSULF: American Journal of Science, v. 314, n. 9, p. 1259–1283, https://doi.org/10.2475/09.2014.01

Saltzman, M. R., and Thomas, E., 2012, Chapter 11 - Carbon Isotope Stratigraphy, *in* The Geologic Time Scale: Boston, Elsevier, p. 207–232, https://doi.org/10.1016/B978-0-444-59425-9.00011-1

Shields, G. A., and Mills, B. J. W., 2017, Tectonic controls on the long-term carbon isotope mass balance: Proceedings of the National Academy of Sciences of the United States of America, v. 114, n. 17, p. 4318–4323, https://doi.org/10.1073/pnas.1614506114

Sim, M. S., Bosak, T., and Ono, S., 2011, Large Sulfur Isotope Fractionation Does Not Require Disproportionation: Science, v. 333, n. 6038, p. 74–77, https://doi.org/10.1126/science.1205103

Sperling, E. A., Wolock, C. J., Morgan, A. S., Gill, B. C., Kunzmann, M., Halverson, G. P., Macdonald, F. A., Knoll, A. H., and Johnston, D. T., 2015, Statistical analysis of iron geochemical data suggests limited late Proterozoic oxygenation: Nature, v. 523, p. 451–454, https://doi.org/10.1038/nature14589

Van Der Meer, D. G., Zeebe, R. E., van Hinsbergen, D. J. J., Sluijs, A., Spakman, W., and Torsvik, T. H., 2014, Plate tectonic controls on atmospheric CO_2 levels since the Triassic: Proceedings of the National

Academy of Sciences of the United States of America, v. 111, n. 12, p. 4380–4385, https://doi.org/10.1073/pnas.1315657111

Veizer, J., Ala, D., Azmy, K., Bruckschen, P., Buhl, D., Bruhn, F., Carden, G. A. F., Diener, A., Ebneth, S., Godderis, Y., Jasper, T., Korte, C., Pawellek, F., Podlaha, O. G., and Strauss, H., 1999, $^{87}Sr/^{86}Sr$, $\delta^{13}C$ and $\delta^{18}O$ evolution of Phanerozoic seawater: Chemical Geology, v. 161, n. 1–3, p. 59–88, https://doi.org/10.1016/S0009-2541(99)00081-9

Wallace, M. W., Hood, A. V. S., Shuster, A., Greig, A., Planavsky, N. J., and Reed, C. P., 2017, Oxygenation history of the Neoproterozoic to early Phanerozoic and the rise of land plants: Earth and Planetary Science Letters, v. 466, p. 12–19, https://doi.org/10.1016/j.epsl.2017.02.046

Watson, A., Lovelock, J. E., and Margulis, L., 1978, Methanogenesis, fires and the regulation of atmospheric oxygen: Biosystems, v. 10, n. 4, p. 293–298, https://doi.org/10.1016/0303-2647(78)90012-6

Wildman, R. A., Jr., Hickey, L. J., Dickinson, M. B., Berner, R. A., Robinson, J. M., Dietrich, M., Essenhigh, R. H., and Wildman, C. B., 2004, Burning of forest materials under late Paleozoic high atmospheric oxygen levels: Geology, v. 32, n. 5, p. 457–460, https://doi.org/10.1130/G20255.1

Wu, N., Farquhar, J., Strauss, H., Kim, S.-T., and Canfield, D. E., 2010, Evaluating the S-isotope fractionation associated with Phanerozoic pyrite burial: Geochimica et Cosmochimica Acta, v. 74, n. 7, p. 2053–2071, https://doi.org/10.1016/j.gca.2009.12.012

Zeebe, R. E., 2012, LOSCAR: Long-term Ocean-atmosphere-Sediment CArbon cycle Reservoir Model v2.0.4: Geoscientific Model Development, v. 5, p. 149–166, https://doi.org/10.5194/gmd-5-149-2012

Zeebe, R. E., and Wolf-Gladrow, D., 2001, CO_2 in seawater: Equilibrium, kinetics, isotopes: Amsterdam, New York, Elsevier Science, Elsevier Oceanographic Series, v. 65, 360 p.